Progress In Electromagnetics Research B, Vol. 14, 341–381, 2009

BOUNDARY EFFECTS IN THE ELECTROMAGNETIC RESPONSE OF A METAMATERIAL IN THE CASE OF NORMAL INCIDENCE

A. D. Scher and E. F. Kuester

Department of Electrical and Computer Engineering
University of Colorado at Boulder
Boulder, CO 80309, USA

Abstract—In this paper we investigate boundary effects and other consequences of spatial dispersion by analyzing in detail the response of a metamaterial half-space to a monochromatic plane wave normally incident from free-space. The metamaterial is composed of an orthorhombic lattice of identical particles, each of which exhibits both an electric and magnetic response. Rather than relying on the conventional boundary conditions and the Clausius-Mossotti equations, we use instead the point-dipole interaction model and an expansion of polarization in eigenmodes to determine the structure's dispersion relation and electromagnetic response. Using the nearest-neighbor approximation, we show how truncating the crystal lattice excites an "ordinary" mode and two "extraordinary" modes that are necessary to satisfy the boundary conditions at the interface. For most cases, the extraordinary modes are evanescent, and thus form a thin transition layer at the surface. However, under certain conditions, typically near particle resonances, either one or both of these modes can be propagating.

1. INTRODUCTION AND BACKGROUND

The variety and capability of devices for microwave and optical applications are determined to a great extent by the materials from which the devices are made. Ordinary materials, however, exhibit only a subset of the material parameters theoretically possible. One possible way to circumvent this limitation is by extending our definition of materials to include artificial structures or metamaterials, which can by

Corresponding author: A. D. Scher (scherad@colorado.edu).

design extend the range of material parameters available. Mimicking the structure of naturally occurring crystals, many metamaterials are composed of an ordered lattice of discrete scatterers or "particles" fashioned out of linear media. Preferably, the feature sizes of the particles and the period of the lattice itself should be on a scale much smaller than the field variation inside the medium so that the composite as a whole can be regarded as an effective medium. In this manner, an effective permittivity and effective permeability can be assigned to the structure whose values would be related to the response and interactions between the individual particles. Ideally, such a description would hold true right up to the boundary of a metamaterial and free-space.

However, at the current state of fabrication, most metamaterials involve inhomogeneities, which, while electrically small, are still sizable compared to a wavelength at the frequency of operation. This means that, as opposed to ordinary media, most metamaterials operate at frequencies above the classical "long-wavelength limit" in which the basic Clausius-Mossotti equations and related assumptions hold valid. On the other hand, metamaterials typically operate at frequencies below the "photonic band gap regime", in which the lattice dimensions are equal to or larger than a half wavelength. Hence, the operation of most practical metamaterials falls in a sort of transitional frequency band, which has been dubbed the "metamaterials regime" [1]. Consequently, the electromagnetic properties of the composite cannot completely be described using a local description. Most notably, particles near a boundary experience a different local-field environment than those in the bulk. This phenomenon of spatial dispersion means that the simple characterization of a boundary in terms of a sharp interface governed by the ordinary boundary conditions is not correct.

In this paper we investigate the surface effects and other consequences of spatial dispersion by analyzing in detail the response of a metamaterial half-space to a monochromatic plane wave normally incident from free-space. Rather than relying on the conventional boundary conditions and the Clausius-Mossotti equations, we use instead the point-dipole interaction model and an expansion of polarization in eigenmodes. This basic analytical technique finds its origins in an influential paper in the field of crystal optics by Mahan and Obermair in which the reflectivity of a semi-infinite dielectric crystal was calculated for the case of normal incidence [2]. They showed how disrupting the periodicity of a crystal lattice through truncation excites a sum of evanescent and/or propagating polariton modes which are necessary to satisfy the boundary conditions at the interface, analogously to how a discontinuity in a waveguide excites higher-order

modes. Each of these modes contributes to the scattered field, which produces a slight deviation from the traditional Fresnel laws. Later, Philpott extended this work to the case of oblique incidence for both semi-infinite crystals [3, 4] and crystals of finite thickness [5].

It is well known that the reactive near-fields (i.e., quasi-static fields) produced by a two-dimensional planar array of oscillating point dipoles decreases rapidly to zero with increasing perpendicular distance from the plane. In the works cited in the previous paragraph, the authors used this fact to simplify their analyses by artificially cutting off the near-field interaction to zero after a certain number of nearest neighbors. For an infinite lattice of electric dipoles in the case of normal incidence, it turns out that cutting off near-field interactions after N nearest neighbors results in $N+1$ independent eigenmodes [2]. In order to deal with this supposedly troubling result, Mead employed the "exp model" in which the interaction between crystal planes is assumed to fall off exponentially with distance. In this way he found the lattice of dipoles supports exactly two eigenmodes - the same number of eigenmodes as the nearest neighbor approximation ($N = 1$) [6]. The following year, Mead formulated a formally closed solution to the problem, which entails evaluating a complicated contour integral [7]. In both of these works, Mead claimed that artificially cutting off nearest neighbor interactions to zero does not always lead to correct results, and therefore does not constitute an appropriate method of analysis. However, this claim is only valid if the spacing between adjacent planes approaches or exceeds that of a free space wavelength, because in such a case the near-field interactions do not fall off fast enough [8]. For a cubic lattice of dipoles, in which the lattice constants are much smaller than a wavelength, it has been suggested that the nearest-neighbor approximation ($N = 1$) is suitable and accurate [9].

In recent years the discrete dipole model, originally developed for actual dielectrics and crystal optics, has been adapted to the analysis of artificial structures and metamaterials. In 2000, Tretyakov and Viitanen [10] essentially re-derived Mahan and Obermair's original results in modern notation by finding the dispersion relation for a lattice of non-magnetic scatterers in the case of normal incidence. The results of this work are only applicable to cases in which the lattice period is sufficiently smaller than a wavelength. This is because the authors used an approximate intraplanar interaction constant describing near-field coupling that, while simple, is only valid at low frequencies (denoted as $\beta(0)$ in [10]). In fact, on careful inspection, the earlier work by Mahan and Obermair is also limited by a similar constraint since they tacitly assumed quasi-static values for near-field coupling (see Table 1 in [2] — the tabulated values are the near-

field interaction constants in the static limit). The main difficulty lies in evaluating the dynamic lattice interaction constant describing the internal fields acting on a dipole produced by every other polarized dipole in the lattice itself; the problem is that the series involved in the calculation exhibits poor convergence and has no known closed-form solution. Yatsenko et al. formulated an elegant but approximate solution to the problem of intraplanar interaction for a single array by explicitly considering discrete interactions from nearby scatterers (within some radius R), while approximating the rest of the array as a polarization sheet minus a hole of the same radius [11]. More recently, Belov and Simovski re-expressed the offending divergent series describing the local-field interaction in terms of a new rapidly convergent series by utilizing the Poisson summation formula and a singularity cancelation technique, and used it to solve for the dispersion relation of both electric and magnetic composites in the case of oblique electromagnetic propagation [12, 13]. The authors also demonstrated that in the static limit the newly derived dynamic interaction constant reduces to the known static interaction constant as developed and presented for artificial dielectrics in Collin's popular textbook [14].

More recently, the basic Mahan-Obermair approach has been expanded by Simovski et al. to the case of a metamaterial with discrete particles exhibiting both electric and magnetic dipole responses [15–18]. In these works, the authors analyze the metamaterial response by invoking the "zero-neighbor approximation", meaning all near-field interactions between planes are ignored. While this approximation is adequate and instructive for investigating bulk effects, accounting for near-field interactions between planes are essential for capturing detailed boundary effects, as demonstrated by Berman for the nonmagnetic case [19]. In the present work we analyze the response of a metamaterial half-space composed of an ordered lattice of electric and magnetic dipoles, akin to the structure studied by Simovski et al. in the references above. However, because we are interested here in accurately modeling and investigating surface effects, we shall go one step further and employ the nearest neighbor approximation. In this manner, we shall discover that the structure supports three polarization modes (compared to only two modes for the nonmagnetic case), which are necessary to satisfy the boundary conditions and give rise to an excess polarization density localized to the surface region. Since our analytical solution is independent of the effective medium description altogether, it can be useful as a benchmark to compare with the various effective medium and surface models proposed in the literature. It is also our hope that this work will promote a better understanding and insight into the problem of scattering from metamaterials in general.

2. PROBLEM FORMULATION

Consider a transverse electromagnetic (TEMz) monochromatic plane wave with wave vector $\boldsymbol{k} = k_0\hat{\boldsymbol{a}}_z$ normally incident from free-space upon a metamaterial half-space composed of a semi-infinite orthorhombic lattice of particles in the region $z \geq 0$, as shown in Fig. 1. The sites of the lattice are taken to be

$$\boldsymbol{R}_{s,l,n} = \hat{\boldsymbol{a}}_x as + \hat{\boldsymbol{a}}_y bl + \hat{\boldsymbol{a}}_z dn, \tag{1}$$

where $s, l = 0, \pm 1, \pm 2, \ldots, n = 0, 1, 2, \ldots$, and a, b, and d are the lattice periods in the x-, y-, and z-directions, respectively. Since we are interested in the structure's electromagnetic response at frequencies below the Bragg diffraction regime, we restrict the dimensions of the lattice to be smaller a wavelength in free-space, i.e., $k_0 \max(a, b, d) < 2\pi$. Note that in the more general case of oblique incidence (not considered here), the dimensions of the lattice would have to be smaller than a half wavelength in free-space to avoid Bragg diffraction.

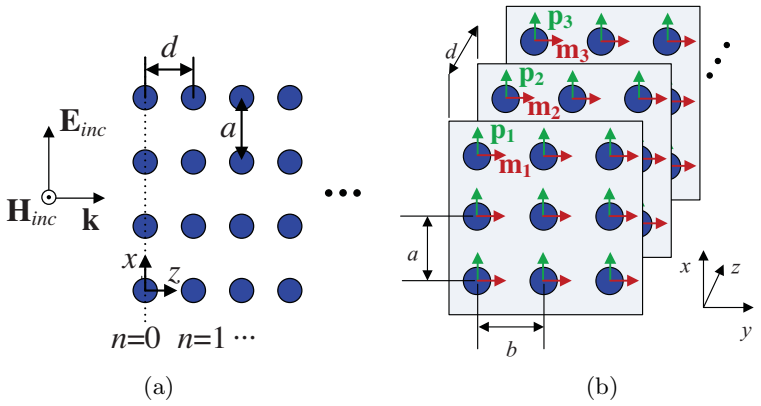

Figure 1. Metamaterial half-space excited by a normally incident plane wave. Shown here are views of the (a) xz-plane cross section and (b) one point perspective in the transverse plane. For convenience, the particles are shown as spheroids. By symmetry of the problem, all particles in plane n have the same electric dipole moment $\boldsymbol{p}_n$ and magnetic dipole moment $\boldsymbol{m}_n$, which are polarized along the directions of the incident electric and magnetic field vectors, respectively.

Following in the tradition of the microscopic model, in this study we use the point-dipole interaction approximation. This means that the fields produced by an individual particle are assumed to be equal to those produced by an oscillating point-dipole located at the center of

the particle. This approximation simplifies the problem considerably in that the responses of the particles are characterized solely by their electric and magnetic polarizability dyadics, denoted $\overline{\overline{\boldsymbol{\alpha}}}_E(\omega)$ and $\overline{\overline{\boldsymbol{\alpha}}}_M(\omega)$, respectively. The point-dipole interaction approximation requires that contributions from higher order multipoles be negligible. Hence, we restrict our analysis to particles with dimensions sufficiently smaller than a wavelength of the fields inside the medium so that the variation of local fields over the volume of the particles can be ignored. As a further simplification, in this work we consider only biaxially anisotropic particles exhibiting no magnetoelectric coupling. This corresponds to polarizability dyadics with non-zero elements exclusively along the diagonal, i.e., $\overline{\overline{\boldsymbol{\alpha}}}_E = \hat{\boldsymbol{a}}_x\hat{\boldsymbol{a}}_x\alpha_E^{xx} + \hat{\boldsymbol{a}}_y\hat{\boldsymbol{a}}_y\alpha_E^{yy} + \hat{\boldsymbol{a}}_z\hat{\boldsymbol{a}}_z\alpha_E^{zz}$ and $\overline{\overline{\boldsymbol{\alpha}}}_M = \hat{\boldsymbol{a}}_x\hat{\boldsymbol{a}}_x\alpha_M^{xx} + \hat{\boldsymbol{a}}_y\hat{\boldsymbol{a}}_y\alpha_M^{yy} + \hat{\boldsymbol{a}}_z\hat{\boldsymbol{a}}_z\alpha_M^{zz}$. These polarizability dyadics characterize the response of a wide range of particles which can be used in the implementation of metamaterials such as single and layered cuboids, ellipsoids, and cylinders fashioned from linear media (including the disk-like resonators recently presented by Wang et al. in [20]). The consideration of more complicated particles such as asymmetrical split-ring resonators which exhibit cross-polarization and magnetoelectric coupling are beyond the scope of this work. Note that the point-dipole interaction approximation requires that the sizes of the particles be sufficiently smaller than the lattice period. For spherical particles, the theory is applicable even as the diameter of the spheres approaches the lattice constant. However, for other particle geometries a more stringent size limit is imposed.

Let us assume that the incident plane wave is polarized along the x-axis, such that the incident electric field $\boldsymbol{E}_{inc}$ and incident magnetic field $\boldsymbol{H}_{inc}$ take the form:

$$\boldsymbol{E}_{inc} = \hat{\boldsymbol{a}}_x E_{inc,x} e^{-jk_0 z} \tag{2}$$

$$\boldsymbol{H}_{inc} = \hat{\boldsymbol{a}}_y \frac{E_{inc,x}}{\eta_0} e^{-jk_0 z}, \tag{3}$$

where $E_{inc,x}$ is the amplitude of the incident electric field and $\eta_0 = \sqrt{\mu_0/\varepsilon_0}$ is the wave impedance of free-space. In the point-dipole approximation, the incident wave excites a distribution of oscillating point-electric and point-magnetic dipole moments situated at the nodes of the lattice, denoted $\boldsymbol{p}_{s,l,n} \equiv \boldsymbol{p}(as, bl, dn)$ and $\boldsymbol{m}_{s,l,n} \equiv \boldsymbol{m}(as, bl, dn)$, respectively. Because the system obeys translational invariance in the xy-plane, the electric and magnetic dipole distributions take the form $\boldsymbol{p}_{s,l,n} = \boldsymbol{p}_n$ and $\boldsymbol{m}_{s,l,n} = \boldsymbol{m}_n$, respectively, where $\boldsymbol{p}_n \equiv \boldsymbol{p}_{n,0,0}$ and $\boldsymbol{m}_n \equiv \boldsymbol{m}_{n,0,0}$ denote the electric and magnetic dipole moments of the particle located at the origin of lattice plane $z = dn,\ n = 1, 2, 3, \ldots$.

In this manner, the total dipole moment distribution of the structure is determined by the distributions $\{\boldsymbol{p}_n\}$ and $\{\boldsymbol{m}_n\}$ in each plane.

3. THE LOCAL-FIELD EQUATIONS AND THE PLANEWISE SUMMATION APPROACH

To find the distributions $\{\boldsymbol{p}_n\}$ and $\{\boldsymbol{m}_n\}$, we write the following local-field equations governing the electromagnetic response of each particle along the z-axis:

$$\boldsymbol{p}_{n'} = \varepsilon_0 \overline{\overline{\boldsymbol{\alpha}}}_E \cdot \boldsymbol{E}_{loc,n'}, \qquad \forall\ n' = 0, 1, 2, \ldots \tag{4}$$

$$\boldsymbol{m}_{n'} = \mu_0^{-1} \overline{\overline{\boldsymbol{\alpha}}}_M \cdot \boldsymbol{B}_{loc,n'}, \quad \forall\ n' = 0, 1, 2, \ldots \tag{5}$$

where $\boldsymbol{E}_{loc,n'}$ and $\boldsymbol{B}_{loc,n'}$ are the respective local-electric and local-magnetic fields acting on the particle located at the origin of lattice plane $z = dn'$. As a major simplification, we note that, due to the translational symmetry in the xy-plane, and because the scatterers are non-chiral and biaxially anisotropic, the induced electric and magnetic dipole moments must be polarized along the same direction as the incident electric and magnetic fields, respectively, i.e., $\boldsymbol{p}_n = \hat{\boldsymbol{a}}_x p_n^{(x)}$ and $\boldsymbol{m}_n = \hat{\boldsymbol{a}}_y m_n^{(y)}$. Hence, our task of finding the plane-to-plane distributions, $\{\boldsymbol{p}_n\}$ and $\{\boldsymbol{m}_n\}$, is equivalent to that of finding the distribution of the two relevant vector components, $\{p_n^{(x)}\}$ and $\{m_n^{(y)}\}$. Consequently, the local-electric and local-magnetic fields must also be polarized along the same directions as the incident electric and magnetic fields, respectively, i.e., $\boldsymbol{E}_{loc,n'} = \hat{\boldsymbol{a}}_x E_{loc,n'}^{(x)}$ and $\boldsymbol{B}_{loc,n'} = \hat{\boldsymbol{a}}_y B_{loc,n'}^{(x)}$. With this, Eqs. (4) and (5) simplify to the following:

$$\boldsymbol{p}_{n'} = \hat{\boldsymbol{a}}_x p_{n'}^{(x)} = \hat{\boldsymbol{a}}_x \varepsilon_0 \alpha_E^{xx} E_{loc,n'}^{(x)}, \qquad \forall\ n' = 0, 1, 2, \ldots \tag{6}$$

$$\boldsymbol{m}_{n'} = \hat{\boldsymbol{a}}_y m_{n'}^{(y)} = \hat{\boldsymbol{a}}_y \mu_0^{-1} \alpha_M^{yy} B_{loc,n'}^{(y)}, \qquad \forall\ n' = 0, 1, 2, \ldots, \tag{7}$$

The local-electric field amplitude $E_{loc,n'}^{(x)}$ is found by superposing the incident electric field at site $(0, 0, n')$ and the induced electric fields produced at that site by all other scatters in the system with indices $(s, l, n) \neq (0, 0, n')$; a dual statement holds for the local-magnetic field amplitude $B_{loc,n'}^{(y)}$. Mathematically, the above statements can be implemented by taking a planewise summation approach, in which

$E^{(x)}_{loc,n'}$ and $B^{(y)}_{loc,n'}$ take following form:

$$E^{(x)}_{loc,n'} = \frac{1}{(ab)^{3/2}\varepsilon_0}\left[\sum_{n=0}^{\infty} p^{(x)}_n C^{\mathrm{TEM}_z,xx}_{n-n'} - \frac{1}{c_0}\sum_{n=0}^{\infty} m^{(y)}_n D^{\mathrm{TEM}_z,xy}_{n-n'}\right] + E_{inc,x}e^{-jk_0dn'} \quad (8)$$

$$B^{(y)}_{loc,n'} = \frac{\mu_0}{(ab)^{3/2}}\left[c_0\sum_{n=0}^{\infty} p^{(x)}_n D^{\mathrm{TEM}_z,yx}_{n-n'} + \sum_{n=0}^{\infty} m^{(y)}_n C^{\mathrm{TEM}_z,yy}_{n-n'}\right] + \mu_0\frac{E_{inc,x}}{\eta_0}e^{-jk_0dn'}, \quad (9)$$

where c_0 is the speed of light in vacuum. The co-field planar interaction constant, denoted $C^{\mathrm{TEM}_z,xx}_{n-n'}(k_0,a,b,d)$ in Eq. (8), quantifies the contribution to the local x-polarized electric field at site $(0,0,n')$ produced by an array of x-polarized electric dipoles located in plane $z = dn$. The co-field planar interaction constant, denoted $C^{\mathrm{TEM}_z,yy}_{n-n'}(k_0,a,b,d)$ in Eq. (9), quantifies the contribution to the local y-polarized B-field at site $(0,0,n')$ produced by an array of y-polarized magnetic dipoles located in plane $z = dn$. In a similar manner, the cross-field planar interaction constants, denoted $D^{\mathrm{TEM}_z,xy}_{n-n'}(k_0,a,b,d)$ in Eq. (8) and $D^{\mathrm{TEM}_z,yx}_{n-n'}(k_0,a,b,d)$ in Eq. (9), quantify magnetic-to-electric coupling and electric-to-magnetic coupling, respectively. We point out that, by construction, both the co-field and cross-field planar interaction constants are dimensionless quantities. The multiplying factors, $(ab)^{-3/2}\varepsilon_0^{-1}$ and $(ab)^{-3/2}\mu_0$, on the right sides of Eqs. (8) and (9), respectively, serve as the normalization factors. To further simplify the problem, we note that due to reciprocity and symmetry, the two cross-field planar interaction constants are the negatives of each other, i.e., $D^{\mathrm{TEM}_z,xy}_{n-n'} = -D^{\mathrm{TEM}_z,yx}_{n-n'}$, and the co-field interaction constants are related by interchanging a and b, i.e., $C^{\mathrm{TEM}_z,yy}_{n-n'}(k_0,a,b,d) = C^{\mathrm{TEM}_z,xx}_{n-n'}(k_0,b,a,d)$. In this manner, only two planar interaction constants are independent in Eqs. (8) and (9), which for our purposes we take to be $C^{\mathrm{TEM}_z,xx}_{n-n'}$ and $D^{\mathrm{TEM}_z,yx}_{n-n'}$.

4. THE PLANAR INTERACTION CONSTANTS

Let us first single out and consider in detail the co-field planar interaction constant, $C^{\mathrm{TEM}_z,xx}_{n-n'}$. By definition, for intraplanar coupling, i.e., $n = n'$, this interaction constant is found by first removing

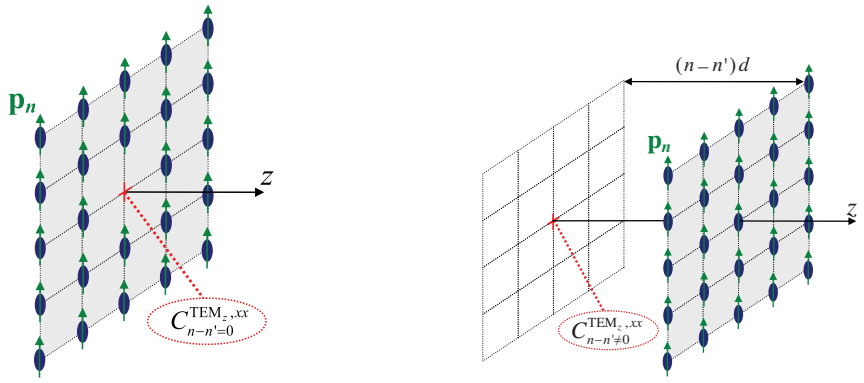

(a) Intraplanar coupling ($n = n'$) (b) Interplanar coupling ($n \neq n'$)

Figure 2. The location of the source dipoles relative to the observation site $(0, 0, n')$ for (a) intraplanar coupling and (b) interplanar coupling.

the dipole from the origin of plane $z = dn'$ and then summing the contribution to the x-polarized electric field (normalized by $(ab)^{-3/2}\varepsilon_0^{-1}$) at the position of the removed dipole as produced by all other x-polarized dipoles (each normalized to have unit strength) within the same plane, i.e.,

$$C_0^{\mathrm{TEM}_z,xx}(k_0, a, b) = \varepsilon_0 (ab)^{3/2} \sum_{(s,l)\neq(0,0)} \hat{\boldsymbol{a}}_x \cdot \overleftrightarrow{\boldsymbol{G}}^{(1)}(\boldsymbol{R}_{s,l,0}) \cdot \hat{\boldsymbol{a}}_x \qquad (10)$$

where the double summation is over all indices s and l except for that corresponding to transverse site $(s, l) = (0, 0)$, $\boldsymbol{R}_{s,l,0} \equiv \hat{\boldsymbol{a}}_x as + \hat{\boldsymbol{a}}_y bl$ is the transverse position vector, and the function $\overleftrightarrow{\boldsymbol{G}}^{(1)}(\boldsymbol{R})$ denotes the dyadic Green's function of free space describing the electric field evaluated at position $\boldsymbol{R} = \hat{\boldsymbol{a}}_x x + \hat{\boldsymbol{a}}_y y + \hat{\boldsymbol{a}}_z z$ as produced by a single electric dipole with arbitrary vector orientation located at the coordinate origin:

$$\overleftrightarrow{\boldsymbol{G}}^{(1)}(\boldsymbol{R}) = \frac{1}{4\pi\varepsilon_0}\left(k_0^2 \overleftrightarrow{I} + \boldsymbol{\nabla}\boldsymbol{\nabla}\right)\frac{e^{-jk_0|\boldsymbol{R}|}}{|\boldsymbol{R}|} \qquad (11)$$

Fig. 2(a) illustrates the location of the source dipoles relative to the observation site $(0, 0, n')$ for the lattice sum in Eq. (10) describing intraplanar coupling. Substituting Eq. (11) for $\overleftrightarrow{\boldsymbol{G}}^{(1)}(\boldsymbol{R})$ into Eq. (10) results in the following simplified expression for $C_0^{\mathrm{TEM}_z,xx}$:

$$C_0^{\mathrm{TEM}_z,xx}(k_0,a,b) = \frac{(ab)^{3/2}}{4\pi} \sum_{(s,l)\neq(0,0)} \left[k_0^2 \frac{e^{-jk_0\sqrt{x^2+y^2+z^2}}}{\sqrt{x^2+y^2+z^2}} + \frac{\partial^2}{\partial x^2}\left(\frac{e^{-jk_0\sqrt{x^2+y^2+z^2}}}{\sqrt{x^2+y^2+z^2}} \right) \right]_{(x,y,z)=(al,bs,0)} \tag{12}$$

A key challenge resides in evaluating the series on the right-hand side of Eq. (12). The problem is that the series has no known closed-form solutions, and is in fact classically divergent for a purely real wavenumber k_0. However, convergence can be secured using the principal of limiting absorption, which entails first adding a small imaginary part to the free space wave number k_0 and then taking the limit $\mathrm{Im}\,[k_0] \to 0$. Using this approach along with the double Poisson summation formula and a singularity cancellation technique, this series has recently been cast by Belov and Simovski [13] into an equivalent series with rapid convergence convenient for numerical calculation:

$$\begin{aligned} C_0^{\mathrm{TEM}_z,xx}(k_0,a,b) = (ab)^{3/2}\mathrm{Re}\Bigg\{ & \frac{-2}{\pi a}\sum_{l=1}^{\infty}\sum_{s=1}^{\infty} p_s^2 K_0(p_s b l) \\ & + \frac{k_0^2}{2a}\sum_{l=1}^{\infty}\left(\frac{2}{g_l b} - \frac{1}{\pi l}\right) + \frac{1}{\pi a^3}\sum_{s=1}^{\infty}\frac{(2jk_0a+3)s+2}{s^3(s+1)(s+2)}e^{-jk_0as} \\ & + \frac{k_0^2}{2a\pi}\left(\ln\frac{k_0 b}{4\pi} + 0.577\right) \\ & + \frac{1}{4\pi a^3}\left[-2(jk_0a+1)\left(t_+^2\ln t_- + e^{jk_0a}\right) - 4jk_0a(t_+\ln t_-) + 3\right]\Bigg\} \\ & + j(ab)^{3/2}\left\{-\frac{k_0}{2ab} + \frac{k_0^3}{6\pi}\right\} \end{aligned} \tag{13}$$

where

$$p_s = \sqrt{\left(\frac{2\pi s}{a}\right)^2 - k_0^2}, \qquad g_l = \sqrt{\left(\frac{2\pi l}{b}\right)^2 - k_0^2},$$
$$t_+ = 1 - e^{jk_0a}, \qquad t_- = 1 - e^{-jk_0a}.$$

and $K_0(x)$ is the zeroth-order modified Bessel function (as defined in section 9.6 in Abramowitz and Stegun [21]). Note that both p_s and g_l are real valued because of our initial assumption that $k_0 \max(a,b,d) < 2\pi$.

For interplanar coupling, i.e., $n \neq n'$, the interaction constant $C_{n-n'}^{\mathrm{TEM}_z,xx}$ is found by summing the contribution to the x-polarized

electric field (normalized by $(ab)^{-3/2}\varepsilon_0^{-1}$) at site $(0,0,n')$ produced by a lattice of x-polarized electric dipoles (each normalized to have unit strength) located in an adjacent plane $z = dn$:

$$C^{\mathrm{TEM}_z,xx}_{n-n'\neq 0}(k_0,a,b,d) = \varepsilon_0 (ab)^{3/2} \sum_{s=-\infty}^{\infty} \sum_{l=-\infty}^{\infty} \hat{\boldsymbol{a}}_x \cdot \overleftrightarrow{\boldsymbol{G}}^{(1)}(\boldsymbol{R}_{s,l,n-n'}) \cdot \hat{\boldsymbol{a}}_x,\ n \neq n' \tag{14}$$

where $\boldsymbol{R}_{s,l,n-n'} \equiv \hat{\boldsymbol{a}}_x as + \hat{\boldsymbol{a}}_y bl + \hat{\boldsymbol{a}}_z d(n-n')$. Fig. 2(b) illustrates the location of the source dipoles relative to the observation site $(0,0,n')$ for the lattice sum in Eq. (14) describing interplanar coupling. Substituting Eq. (11) for $\overleftrightarrow{\boldsymbol{G}}^{(1)}(\boldsymbol{R})$ into Eq. (14) results in the following expression for $C^{\mathrm{TEM}_z,xx}_{n-n'\neq 0}$:

$$C^{\mathrm{TEM}_z,xx}_{n-n'\neq 0}(k_0,a,b,d) = \frac{(ab)^{3/2}}{4\pi} \sum_{s=-\infty}^{\infty} \sum_{l=-\infty}^{\infty} \left[k_0^2 \frac{e^{-jk_0\sqrt{x^2+y^2+z^2}}}{\sqrt{x^2+y^2+z^2}} + \frac{\partial^2}{\partial x^2} \left(\frac{e^{-jk_0\sqrt{x^2+y^2+z^2}}}{\sqrt{x^2+y^2+z^2}} \right) \right]_{(x,y,z)=(al,bs,d(n-n'))} \tag{15}$$

Using the principal of limiting absorption with the double Poisson summation formula, we can rewrite Eq. (15) as the following expansion of Floquet harmonics [8, 13]:

$$C^{\mathrm{TEM}_z,xx}_{n-n'\neq 0}(k_0,a,b,d) = \frac{-j(ab)^{1/2}}{2} \sum_{l=-\infty}^{\infty} \sum_{s=-\infty}^{\infty} \left(\frac{k_0^2 - (2\pi s/a)^2}{k^z_{s,l}} \right) e^{-j(|n-n'|dk^z_{s,l})},\ n \neq n' \tag{16}$$

where the wavenumbers of the individual Floquet harmonics are given by $k^z_{s,l} = \sqrt{(2\pi s/a)^2 + (2\pi l/b)^2 - k_0^2}$. Here we choose the root of $k^z_{s,l}$ such that $\mathrm{Im}(\sqrt{\cdot}) < 0$. Note that if $k_0 \max(a,b) < 2\pi$ then $k^z_{s,l}$ is purely negative imaginary for all terms in the series expansion with indices $(s,l) \neq (0,0)$, i.e., $k^z_{(s,l)\neq(0,0)} = -j|k^z_{(s,l)\neq(0,0)}|$. It follows that the corresponding terms in the series expansion in Eq. (16) decay rapidly to zero with increasing interplanar distance $|n-n'|d$. Physically, these terms are associated with the cut-off or evanescent free-space modes produced by a two-dimensional array of dipoles, and define the reactive near-field in the free-space region surrounding the array. On the other hand, the zeroth-order term, corresponding to index $(s,l) = (0,0)$, with wavenumber $k^z_{0,0} = k_0$, does not decay. This term is associated with the propagating free-space mode produced by a two-dimensional

array of dipoles. Thus, for large interplanar distances $|n - n'|d$, the zeroth-order term is dominant in the series expansion on the right-hand side of Eq. (16).

With this in mind, we shall find it advantageous to expand $C_{n-n'}^{\mathrm{TEM}_z,xx}$ as a sum of two components, describing separately short-range (SR) and long-range (LR) interactions:

$$C_{n-n'}^{\mathrm{TEM}_z,xx}(k_0,a,b,d) \equiv C_{n-n',\mathrm{SR}}^{\mathrm{TEM}_z,xx}(k_0,a,b,d) + C_{n-n',\mathrm{LR}}^{\mathrm{TEM}_z,xx}(k_0,a,b,d) \tag{17}$$

where the respective SR and LR components of $C_{n-n'}^{\mathrm{TEM}_z,xx}$ are recognized from Eqs. (13) and (16) to be:

$$C_{n-n',\mathrm{LR}}^{\mathrm{TEM}_z,xx}(k_0,a,b,d) = -j\frac{k_0(ab)^{1/2}}{2}e^{-j|n-n'|k_0 d} \tag{18}$$

$$C_{n-n',\mathrm{SR}}^{\mathrm{TEM}_z,xx}(k_0,a,b,d) = \begin{cases} \displaystyle\sum_{(s,l)\neq(0,0)} \frac{(ab)^{1/2}\left[k_0^2-(2\pi s/a)^2\right]}{2k_{s,l}^z} e^{-|n-n'|dk_{s,l}^z}, & n \neq n' \\ \mathrm{RE}\left\{C_0^{\mathrm{TEM}_z,xx}\right\} + j(ab)^{3/2}\frac{k_0^3}{6\pi}, & n = n' \end{cases} \tag{19}$$

where $k_{s,l}^z$ is defined in the comments following Eq. (16) and $C_0^{\mathrm{TEM}_z,xx}$ is given by Eq. (13). In formulating Eqs. (17)–(19), we used the fact that from Eq. (13) the imaginary part of $C_0^{\mathrm{TEM}_z,xx}$ is equal to:

$$\mathrm{Im}\left\{C_0^{\mathrm{TEM}_z,xx}(k_0,a,b)\right\} = (ab)^{3/2} j\left\{\frac{k_0^3}{6\pi} - \frac{k_0}{2ab}\right\}. \tag{20}$$

Additionally, by construction, the so-called radiation damping term $j(ab)^{3/2}k_0^3/6\pi$ is included as a short-range effect in Eq. (19) and will end up compensating for dipole radiation losses as we shall see in the next section. By the identity $C_{n-n'}^{\mathrm{TEM}_z,yy}(k_0,a,b,d) = C_{n-n'}^{\mathrm{TEM}_z,xx}(k_0,b,a,d)$, it follows that we can also expand $C_{n-n'}^{\mathrm{TEM}_z,yy}$ as a sum of two components describing separately short-range (SR) and long-range (LR) interactions, i.e., $C_{n-n'}^{\mathrm{TEM}_z,yy} \equiv C_{n-n',\mathrm{SR}}^{\mathrm{TEM}_z,yy} + C_{n-n',\mathrm{LR}}^{\mathrm{TEM}_z,yy}$. From Eq. (18) we see that the long-range component of $C_{n-n'}^{\mathrm{TEM}_z,xx}$ is invariant with respect to the interchange of variables a and b, i.e., $C_{n-n',\mathrm{LR}}^{\mathrm{TEM}_z,xx}(k_0,a,b,d) = C_{n-n',\mathrm{LR}}^{\mathrm{TEM}_z,xx}(k_0,b,a,d)$. Hence, the long-range components of $C_{n-n'}^{\mathrm{TEM}_z,yy}$ and $C_{n-n'}^{\mathrm{TEM}_z,xx}$ are equal, i.e., $C_{n-n',\mathrm{LR}}^{\mathrm{TEM}_z,yy} =$

$C^{\mathrm{TEM}_z,xx}_{n-n',\mathrm{LR}}$. On the other hand, the short range components of $C^{\mathrm{TEM}_z,yy}_{n-n'}$ and $C^{\mathrm{TEM}_z,xx}_{n-n'}$ are only equal in the case of a square lattice ($a = b$).

In an analogous fashion we can also expand the cross-field planar interaction constant $D^{\mathrm{TEM}_z,yx}_{n-n'}$ as a sum of two components, describing separately short-range (SR) and long-range (LR) interactions:

$$D^{\mathrm{TEM}_z,yx}_{n-n'}(k_0,a,b,d) \equiv D^{\mathrm{TEM}_z,yx}_{n-n',\mathrm{SR}}(k_0,a,b,d) + D^{\mathrm{TEM}_z,yx}_{n-n',\mathrm{LR}}(k_0,a,b,d) \tag{21}$$

where the respective SR and LR components of $D^{\mathrm{TEM}_z,yx}_{n-n'}$ are (see [22] for details):

$$D^{\mathrm{TEM}_z,yx}_{n-n',\mathrm{LR}}(k_0,a,b,d) = \mathrm{sgn}(n-n')\frac{jk_0(ab)^{1/2}}{2}e^{-j|n-n'|k_0 d} \tag{22}$$

$$D^{\mathrm{TEM}_z,yx}_{n-n',\mathrm{SR}}(k_0,a,b,d) = \mathrm{sgn}(n-n')\frac{jk_0(ab)^{1/2}}{2}\sum_{(s,l)\neq(0,0)} e^{-|n-n'|dk^z_{s,l}} \tag{23}$$

where $\mathrm{sgn}(x)$ is the signum function ($\mathrm{sgn}(x) = 1$ for $x > 0$, $\mathrm{sgn}(x) = -1$ for $x < 0$, and $\mathrm{sgn}(x) = 0$ for $x = 0$). Note that for intraplanar coupling ($n = n'$), the cross-field coupling term $D^{\mathrm{TEM}_z,yx}_{n-n'}$ is equal to zero.

The planar interaction constants corresponding to various planar indices are calculated and tabulated in Table 1 for (*i*) a cubic lattice, $a = b = d$, and rectangular lattices with lattice proportions (*ii*) $a = b$, $d = 2a$, and (*iii*) $a = b$, $d = a/2$. For all three geometries, we choose the operating frequency such that $k_0 a = 0.1$. In evaluating Eqs. (18), (19), (22), and (23) used to generate Table 1, we took twenty terms in each series, in which we estimate the truncation error to be better than 0.001% for each.

A key feature of Table 1 is that the short range terms, $C^{\mathrm{TEM}_z,xx}_{n-n',\mathrm{SR}}$ and $D^{\mathrm{TEM}_z,yx}_{n-n',\mathrm{SR}}$, decrease to zero very rapidly with increasing separation distance $|n-n'|d$. This means that when solving Eqs. (6) and (7) with Eqs. (8) and (9), we can neglect SR interactions after a finite number of lattice planes. Guided by Table 1 (*i*) and (*ii*) we conclude that if the lattice period along the normal is equal to or larger than the period along the transverse directions (i.e., $d \geq \max(a,b)$), then the SR co-field planar interaction term, $C^{\mathrm{TEM}_z,xx}_{n-n',\mathrm{SR}}$, is negligible and can be set equal to zero for $|n-n'| \geq 2$ with little loss of accuracy. We also conclude that the SR cross-field planar interaction term $D^{\mathrm{TEM}_z,yx}_{n-n',\mathrm{SR}}$ is negligible for all planar indices. Therefore, this term can simply be set to zero altogether. Substituting Eqs. (8) and (9) into Eqs. (6) and (7) and utilizing these two approximations results in the following form of

Table 1. Values of the planar interaction constants for $k_0 a = 0.1$.

(*i*) Cubic lattice (*a* = *b* = *d*)

Plane index n-n'	$\left\lvert C^{\mathrm{TEM}_z,xx}_{n-n',\mathrm{LR}}\right\rvert$	$C^{\mathrm{TEM}_z,xx}_{n-n',\mathrm{SR}}$	$\left\lvert D^{\mathrm{TEM}_z,yx}_{n-n',\mathrm{LR}}\right\rvert$	$D^{\mathrm{TEM}_z,yx}_{n-n',\mathrm{SR}}$
0	0.05	0.3571	0	0
1	0.05	-0.013	0.05	$j4.03\times10^{-4}$
2	0.05	-2.21×10^{-5}	0.05	$j7.02\times10^{-7}$
3	0.05	-4.1×10^{-8}	0.05	$j1.3\times10^{-9}$
4	0.05	-7.67×10^{-11}	0.05	$j2.4\times10^{-12}$

(*ii*) Non-cubic lattice I (*a* = *b*, *d*=2*a*)

Plane index n-n'	$\left\lvert C^{\mathrm{TEM}_z,xx}_{n-n',\mathrm{LR}}\right\rvert$	$C^{\mathrm{TEM}_z,xx}_{n-n',\mathrm{SR}}$	$\left\lvert D^{\mathrm{TEM}_z,yx}_{n-n',\mathrm{LR}}\right\rvert$	$D^{\mathrm{TEM}_z,yx}_{n-n',\mathrm{SR}}$
0	0.05	0.3571	0	0
1	0.05	-2.2×10^{-5}	0.05	$j7.02\times10^{-7}$
2	0.05	-7.66×10^{-11}	0.05	$j2.44\times10^{-12}$
3	0.05	-2.68×10^{-16}	0.05	$j8.52\times10^{-18}$
4	0.05	-9.35×10^{-22}	0.05	$j3\times10^{-23}$

(*iii*) Non-cubic lattice II (*a* = *b*, *d*=*a*/2)

Plane index n-n'	$\left\lvert C^{\mathrm{TEM}_z,xx}_{n-n',\mathrm{LR}}\right\rvert$	$C^{\mathrm{TEM}_z,xx}_{n-n',\mathrm{SR}}$	$\left\lvert D^{\mathrm{TEM}_z,yx}_{n-n',\mathrm{LR}}\right\rvert$	$D^{\mathrm{TEM}_z,yx}_{n-n',\mathrm{SR}}$
0	0.05	0.3571	0	0
1	0.05	-0.4313	0.05	$j0.0118$
2	0.05	-0.013	0.05	$j4.025\times10^{-4}$
3	0.05	-5.22×10^{-4}	0.05	$j1.65\times10^{-5}$
4	0.05	-2.21×10^{-5}	0.05	$j7.02\times10^{-7}$

the local-field equations:

$$p^{(x)}_{n'} = \frac{\alpha^{xx}_E}{(ab)^{3/2}}\left[\sum_{n=0}^{\infty} p^{(x)}_n C^{\mathrm{TEM}_z,xx}_{n-n',\mathrm{LR}} + \sum_{n=n'-1}^{n'+1} p^{(x)}_n C^{\mathrm{TEM}_z,xx}_{n-n',\mathrm{SR}} + \frac{1}{c_0}\sum_{n=0}^{\infty} m^{(y)}_n D^{\mathrm{TEM}_z,yx}_{n-n',\mathrm{LR}}\right] + \alpha^{xx}_E \varepsilon_0 E_{inc,x} e^{-jk_0 dn'},\ \forall\ n' = 0,1,2,\ldots \tag{24}$$

$$m^{(y)}_{n'} = \frac{\alpha^{yy}_M}{(ab)^{3/2}}\left[c_0\sum_{n=0}^{\infty} p^{(x)}_n D^{\mathrm{TEM}_z,yx}_{n-n',\mathrm{LR}} + \sum_{n=0}^{\infty} m^{(y)}_n C^{\mathrm{TEM}_z,xx}_{n-n',\mathrm{LR}} + \sum_{n=n'-1}^{n'+1} m^{(y)}_n C^{\mathrm{TEM}_z,yy}_{n-n',\mathrm{SR}}\right] + \alpha^{yy}_M \frac{E_{inc,x}}{\eta_0} e^{-jk_0 dn'},\ \forall\ n' = 0,1,2,\ldots \tag{25}$$

where in writing Eq. (25) we have invoked the identity, $C^{\mathrm{TEM}_z,yy}_{n-n',\mathrm{LR}} = C^{\mathrm{TEM}_z,xx}_{n-n',\mathrm{LR}}$. For the rest of the paper we assume for simplicity that $d \geq \max(a,b)$ and that Eqs. (24) and (25) hold valid. In contrast, as Table 1 (*iii*) suggests, if the lattice period along the normal is smaller compared to the transverse directions (i.e., $d < \max(a,b)$) then the SR interactions fall off more slowly with increasing separation distance $|n-n'|d$, and, consequently, additional SR terms may be required. It is straightforward to generalize the analysis presented here to include such extra terms.

5. EIGENMODE SOLUTION FOR THE METAMATERIAL HALF-SPACE

Eqs. (24) and (25) constitute an infinite system of coupled equations in an infinite number of variables $p^{(x)}_{n'}$ and $m^{(y)}_{n'}$, $n' = 0, 1, 2, \ldots$. To solve this system of equations we use an expansion of polarization by eigenmodes:

$$p^{(x)}_n = \sum_i P_{x,i} e^{-jq_{z,i}dn} \tag{26}$$

$$m^{(y)}_n = \sum_i M_{y,i} e^{-jq_{z,i}dn} \tag{27}$$

where $P_{x,i}$ and $M_{y,i}$ are the amplitudes of the eigenmodes corresponding to wavenumbers $q_{z,i}$. Each eigenmode (or Floquet wave) constitutes a "natural" solution which can independently propagate through the infinite periodic structure with wavenumber $q_{z,i}$. This was demonstrated to be true for non-magnetic crystals in [2, 8]. In the present work, we will derive the dispersion relation for $q_{z,i}$ by first substituting the form of the solution given by Eqs. (26) and (27) into the inhomogeneous local-field Eqs. (24) and (25) governing the half-space response to a normally incident plane wave. By employing self consistency, the homogeneous components of the local-field equations will be extracted, which describe the natural response of the structure and yield the dispersion relation giving insights into the location of the pass-bands and stop-bands as well as the number of eigenmodes the structure can support. This approach is similar to that undertaken by Philpott in his analysis of a non-magnetic crystalline half-space [4]. In a later section, we shall further demonstrate that the magnetic-to-electric amplitude ratio is fixed for each mode, which we shall denote $B^{\mathrm{TEM}_z}_{yx,i} \equiv M_{y,i}/(c_0 P_{x,i})$. Because this ratio is fixed, there is only one independent parameter governing the amplitude for each mode,

which we shall take to be the electric amplitude, $P_{x,i}$. The particular amplitudes of the eigenmodes are contained in the forced response and are to be determined.

Substituting Eqs. (26) and (27) into Eqs. (24) and (25) leads to the following set of coupled equations:

$$\begin{aligned}\sum_i P_{x,i}e^{-jq_{z,i}dn'} &= \frac{\alpha_E^{xx}}{(ab)^{3/2}}\left[\sum_i P_{x,i}\left[\sum_{n=0}^{\infty} e^{-jq_{z,i}dn}C^{\mathrm{TEM}_z,xx}_{n-n',\mathrm{LR}} + \sum_{n=n'-1}^{n'+1} e^{-jq_{z,i}dn}C^{\mathrm{TEM}_z,xx}_{n-n',\mathrm{SR}}\right]\right] \\ &\quad + \frac{\alpha_E^{xx}}{(ab)^{3/2}}\left[\frac{1}{c_0}\sum_i M_{y,i}\left[\sum_{n=0}^{\infty} e^{-jq_{z,i}dn}D^{\mathrm{TEM}_z,yx}_{n-n',\mathrm{LR}}\right]\right] \\ &\quad + \alpha_E^{xx}\varepsilon_0 E_{inc,x}e^{-jk_0dn'}, \quad \forall\ n' = 0,1,2,\ldots \qquad (28)\end{aligned}$$

$$\begin{aligned}\sum_i M_{y,i}e^{-jq_{z,i}dn'} &= \frac{\alpha_M^{yy}}{(ab)^{3/2}}\left[c_0\sum_i P_{x,i}\left[\sum_{n=0}^{\infty} e^{-jq_{z,i}dn}D^{\mathrm{TEM}_z,yx}_{n-n',\mathrm{LR}}\right]\right] \\ &\quad + \frac{\alpha_M^{yy}}{(ab)^{3/2}}\left[\sum_i M_{y,i}\left[\sum_{n=0}^{\infty} e^{-jq_{z,i}dn}C^{\mathrm{TEM}_z,xx}_{n-n',\mathrm{LR}} + \sum_{n=n'-1}^{n'+1} e^{-jq_{z,i}dn}C^{\mathrm{TEM}_z,yy}_{n-n',\mathrm{SR}}\right]\right] \\ &\quad + \alpha_M^{yy}\frac{E_{inc,x}e^{-jk_0dn'}}{\eta_0}, \quad \forall\ n' = 0,1,2,\ldots \qquad (29)\end{aligned}$$

We proceed next by explicitly evaluating in closed-form the planewise sums over n which appear in Eqs. (28) and (29). First, let us expand the sums involving SR interactions:

$$\begin{aligned}\sum_{n=n'-1}^{n'+1} e^{-jq_{z,i}dn}C^{\mathrm{TEM}_z,xx}_{n-n',\mathrm{SR}} &= e^{-jq_{z,i}dn'}\left[\tilde{C}^{\mathrm{TEM}_z,xx}_{0,\mathrm{SR}} + 2C^{\mathrm{TEM}_z,xx}_{1,\mathrm{SR}}\cos(q_{z,i}d)\right] \\ &\quad - \delta_{n'0}C^{\mathrm{TEM}_z,xx}_{1,\mathrm{SR}}e^{+jq_{z,i}d} + j(ab)^{3/2}\frac{k_0^3}{6\pi}e^{-jq_{z,i}dn'} \qquad (30)\end{aligned}$$

$$\begin{aligned}\sum_{n=n'-1}^{n'+1} e^{-jq_{z,i}dn}C^{\mathrm{TEM}_z,yy}_{n-n',\mathrm{SR}} &= e^{-jq_{z,i}dn'}\left[\tilde{C}^{\mathrm{TEM}_z,yy}_{0,\mathrm{SR}} + 2C^{\mathrm{TEM}_z,yy}_{1,\mathrm{SR}}\cos(q_{z,i}d)\right] \\ &\quad - \delta_{n'0}C^{\mathrm{TEM}_z,yy}_{1,\mathrm{SR}}e^{+jq_{z,i}d} + j(ab)^{3/2}\frac{k_0^3}{6\pi}e^{-jq_{z,i}dn'}, \qquad (31)\end{aligned}$$

where we have defined $\tilde{C}_{0,\mathrm{SR}}^{\mathrm{TEM}_z,xx(yy)} \equiv C_{0,\mathrm{SR}}^{\mathrm{TEM}_z,xx(yy)} - j(ab)^{3/2}k_0^3/6\pi = \mathrm{Re}(C_0^{\mathrm{TEM}_z,xx(yy)})$ and δ_{ij} is the Kronecker delta function ($\delta_{ij} = 1$ for $i = j$ and $\delta_{ij} = 0$ for $i \neq j$). Now let us single out the planewise sum over n involving $C_{n-n',\mathrm{LR}}^{\mathrm{TEM}_z,xx}$ which appears in both Eqs. (28) and (29):

$$\sum_{n=0}^{\infty} e^{-jq_{z,i}dn} C_{n-n',\mathrm{LR}}^{\mathrm{TEM}_z,xx} = -j\frac{k_0(ab)^{1/2}}{2} \sum_{n=0}^{\infty} e^{-jq_{z,i}dn} e^{-j|n-n'|k_0 d} \tag{32}$$

where we have substituted Eq. (18) for $C_{n-n',\mathrm{LR}}^{\mathrm{TEM}_z,xx}$. We see that this sum involves a geometric series, which can be evaluated exactly by assuming that the imaginary part of the wavenumber $q_{z,i}$ is negative. However, if the wavenumber $q_{z,i}$ is purely real, the series can still be evaluated by adding a small imaginary part to the free space wavenumber k_0 such that convergence is secured, and then taking the limit $\mathrm{Im}[k_0] \to 0$ (i.e., invoking the principle of limiting absorption). Both assumptions lead to the same result:

$$\begin{aligned}
\sum_{n=0}^{\infty} e^{-jq_{z,i}dn} e^{-j|n-n'|k_0 d} &= \sum_{n=0}^{n'} e^{-jq_{z,i}dn} e^{-j(n'-n)k_0 d} \\
&\quad + \sum_{n=n'+1}^{\infty} e^{-jq_{z,i}an} e^{-j(n-n')k_0 d} \\
&= e^{-jk_0 dn'} \sum_{n=0}^{n'} e^{-j(q_{z,i}-k_0)dn} + e^{-j[(k_0+q_{z,i})+q_{z,i}n']d} \sum_{n=0}^{\infty} e^{-j(q_{z,i}+k_0)dn} \\
&= e^{-jk_0 dn'} \left[\frac{1-e^{-j(q_{z,i}-k_0)d(n'+1)}}{1-e^{-j(q_{z,i}-k_0)d}}\right] + e^{-j[(k_0+q_{z,i})+q_{z,i}n']d} \left[\frac{1}{1-e^{-j(q_{z,i}+k_0)d}}\right] \\
&= e^{-jk_0 dn'} \left[\frac{1}{1-e^{-j(q_{z,i}-k_0)d}}\right] + e^{-jq_{z,i}dn'} \left[\frac{j\sin(k_0 d)}{\cos(k_0 d) - \cos(q_{z,i}d)}\right]
\end{aligned} \tag{33}$$

where the final expression has been purposely expressed as a sum of two terms; one term proportional to $e^{-jk_0 dn'}$ and the other term proportional to $e^{-jq_{z,i}dn'}$. The rationale for this separation of terms will be apparent shortly. Substituting Eq. (33) into Eq. (32) yields the following closed-form expression:

$$\sum_{n=0}^{\infty} e^{-jq_{z,i}dn} C_{n-n',\mathrm{LR}}^{\mathrm{TEM}_z,xx} = e^{-jk_0 dn'} \left(-j\frac{k_0(ab)^{1/2}}{2}\right) \left[\frac{1}{1-e^{-j(q_{z,i}-k_0)d}}\right]$$

$$+e^{-jq_{z,i}dn'}\left(-j\frac{k_0(ab)^{1/2}}{2}\right)\left[\frac{j\sin(k_0d)}{\cos(k_0d)-\cos(q_{z,i}d)}\right] \quad (34)$$

Next, let us single out the planewise sum over n involving $D^{\mathrm{TEM}_z,yx}_{n-n',\mathrm{LR}}$ which appears in both Eqs. (28) and (29):

$$\sum_{n=0}^{\infty}e^{-jq_{z,i}dn}D^{\mathrm{TEM}_z,yx}_{n-n',\mathrm{LR}}=\frac{jk_0(ab)^{1/2}}{2}\sum_{n=0}^{\infty}\mathrm{sgn}(n-n')e^{-jq_{z,i}dn}e^{-j|n-n'|k_0d} \quad (35)$$

where we have substituted Eq. (22) for $D^{\mathrm{TEM}_z,yx}_{n-n',\mathrm{LR}}$. By again invoking the principal of limiting absorption, this sum can be evaluated in closed form:

$$\begin{aligned}
\sum_{n=0}^{\infty}\mathrm{sgn}(n-n')e^{-jq_{z,i}dn}e^{-j|n-n'|k_0d} &= -\sum_{n=0}^{n'-1}e^{-jq_{z,i}dn}e^{-j(n-n')k_0d}\\
&\quad+\sum_{n=n'+1}^{\infty}e^{-jq_{z,i}dn}e^{-j(n-n')k_0d}\\
&=-e^{-jk_0dn'}\sum_{n=0}^{n'-1}e^{-j(q_{z,i}-k_0)dn}+e^{-j[(k_0+q_{z,i})+q_{z,i}n']d}\sum_{n=0}^{\infty}e^{-j(q_{z,i}+k_0)dn}\\
&=-e^{-jk_0dn'}\left[\frac{1-e^{-j(q_{z,i}-k_0)dn'}}{1-e^{-j(q_{z,i}-k_0)d}}\right]+e^{-j[(k_0+q_{z,i})+q_{z,i}n']d}\left[\frac{1}{1-e^{-j(q_{z,i}+k_0)d}}\right]\\
&=-e^{-jk_0dn'}\left[\frac{1}{1-e^{-j(q_{z,i}-k_0)d}}\right]+e^{-jq_{z,i}dn'}\left[\frac{-j\sin(q_{z,i}d)}{\cos(k_0d)-\cos(q_{z,i}d)}\right] \quad (36)
\end{aligned}$$

Substituting Eq. (36) into Eq. (35) yields the following closed-form expression:

$$\begin{aligned}
\sum_{n=0}^{\infty}e^{-jq_{z,i}an}D^{\mathrm{TEM}_z,yx}_{n-n',\mathrm{LR}} &= e^{-jk_0dn'}\left(\frac{-jk_0(ab)^{1/2}}{2}\right)\left[\frac{1}{1-e^{-j(q_{z,i}-k_0)d}}\right]\\
&\quad+e^{-jq_{z,i}dn'}\left(\frac{jk_0(ab)^{1/2}}{2}\right)\left[\frac{-j\sin(q_{z,i}d)}{\cos(k_0d)-\cos(q_{z,i}d)}\right] \quad (37)
\end{aligned}$$

Finally, substituting Eqs. (30), (31), (34), and (37) into Eqs. (24) and

(25) yields the following expanded form of the local-field equations:

$$
\begin{aligned}
0 \;=\; & \sum_i P_{x,i} \left\{ -e^{+jq_{z,i}d}\delta_{n'0} \frac{C_{1,\mathrm{SR}}^{\mathrm{TEM}_z,xx}}{(ab)^{3/2}} + e^{-jk_0dn'} \left(-j\frac{k_0}{2ab}\right) \right. \\
& \left(\frac{1}{1-e^{-j(q_{z,i}-k_0)d}}\right) + \frac{e^{-jq_{z,i}dn'}}{(ab)^{3/2}} \left[\tilde{C}_{0,\mathrm{SR}}^{\mathrm{TEM}_z,xx} + 2C_{1,\mathrm{SR}}^{\mathrm{TEM}_z,xx} \cos(q_{z,i}d) \right. \\
& \left. \left. - (ab)^{3/2}(\alpha_E^{xx})^{-1} + \frac{j(ab)^{3/2}k_0^3}{6\pi} + \left(\frac{k_0}{2ab}\right) \left(\frac{\sin(k_0d)}{\cos(k_0d)-\cos(q_{z,i}d)}\right) \right] \right\} \\
& -\frac{1}{c_0} \sum_i M_{y,i} \left\{ e^{-jk_0dn'} \left(\frac{jk_0}{2ab}\right) \left[\frac{1}{1-e^{-j(q_{z,i}-k_0)d}}\right] \right. \\
& \left. - e^{-jq_{z,i}dn'} \left(\frac{k_0}{2ab}\right) \left[\frac{\sin(q_{z,i}d)}{\cos(k_0d)-\cos(q_{z,i}d)}\right] \right\} \\
& + \varepsilon_0 E_{inc,x} e^{-jk_0dn'}, \quad \forall\; n' = 0,1,2,\ldots
\end{aligned} \tag{38}
$$

and

$$
\begin{aligned}
0 \;=\; & -c_0 \sum_i P_{x,i} \left\{ e^{-jk_0dn'} \left(\frac{jk_0}{2ab}\right) \right. \\
& \left. \left[\frac{1}{1-e^{-j(q_{z,i}-k_0)d}}\right] - e^{-jq_{z,i}dn'} \left(\frac{k_0}{2ab}\right) \left[\frac{\sin(q_{z,i}d)}{\cos(k_0d)-\cos(q_{z,i}d)}\right] \right\} \\
& + \sum_i M_{y,i} \left\{ -e^{+jq_{z,i}d}\delta_{n'0} C_{1,\mathrm{SR}}^{\mathrm{TEM}_z,yy} + e^{-jk_0dn'} \left(-j\frac{k_0}{2(ab)^{1/2}}\right) \right. \\
& \left(\frac{1}{1-e^{-j(q_{z,i}-k_0)d}}\right) + \frac{e^{-jq_{z,i}dn'}}{(ab)^{3/2}} \left[\tilde{C}_{0,\mathrm{SR}}^{\mathrm{TEM}_z,yy} + 2C_{1,\mathrm{SR}}^{\mathrm{TEM}_z,yy} \cos(q_{z,i}d) \right. \\
& \left. \left. - (ab)^{3/2}(\alpha_M^{yy})^{-1} + \frac{j(ab)^{3/2}k_0^3}{6\pi} + \left(\frac{k_0}{2ab}\right) \left(\frac{\sin(k_0d)}{\cos(k_0d)-\cos(q_{z,i}d)}\right) \right] \right\} \\
& + \frac{E_{inc,x}e^{-jk_0dn'}}{\eta_0}, \quad \forall\; n' = 0,1,2,\ldots
\end{aligned} \tag{39}
$$

We emphasize that Eqs. (38) and (39) hold valid for all planar indices ($n' = 0,1,2,\ldots$). Because both $q_{z,i}$ and k_0 are independent of n', this requires that each group of terms proportional to $e^{-jk_0dn'}$ and $e^{-jq_{z,i}dn'}$ appearing in these equations must separately equal zero (assuming $q_{z,i} \neq k_0$). Performing such a grouping leads to the following five

separate equations:

$$\sum_i P_{x,i} e^{-jq_{z,i}dn'} \left\{ \frac{\tilde{C}_{0,\mathrm{SR}}^{\mathrm{TEM}_z,xx}}{(ab)^{3/2}} + \frac{2C_{1,\mathrm{SR}}^{\mathrm{TEM}_z,xx}}{(ab)^{3/2}} \cos(q_{z,i}d) - \left(\alpha_E^{'xx}\right)^{-1} + \left(\frac{k_0}{2ab}\right)\left(\frac{\sin(k_0 d)}{\cos(k_0 d) - \cos(q_{z,i}d)}\right)\right\}$$
$$+ \sum_i M_{y,i} e^{-jq_{z,i}dn'} \left\{ \frac{1}{c_0}\left(\frac{k_0}{2ab}\right)\left(\frac{\sin(q_{z,i}d)}{\cos(k_0 d) - \cos(q_{z,i}d)}\right)\right\} = 0 \quad (40)$$

$$\sum_i P_{x,i} e^{-jq_{z,i}dn'} \left\{ \frac{c_0\left(\frac{k_0}{2ab}\right)\sin(q_{z,i}d)}{\cos(k_0 d) - \cos(q_{z,i}d)} \right\}$$
$$+ \sum_i M_{y,i} e^{-jq_{z,i}dn'} \left\{ \frac{\tilde{C}_{0,\mathrm{SR}}^{\mathrm{TEM}_z,yy}}{(ab)^{3/2}} + \frac{2C_{1,\mathrm{SR}}^{\mathrm{TEM}_z,yy}}{(ab)^{3/2}} \cos(q_{z,i}d) - \left(\alpha_M^{'yy}\right)^{-1} + \left(\frac{k_0}{2ab}\right)\left(\frac{\sin(k_0 d)}{\cos(k_0 d) - \cos(q_{z,i}d)}\right)\right\} = 0 \quad (41)$$

$$\sum_i P_{x,i} e^{+jq_{z,i}d} = 0 \quad (42)$$

$$\sum_i M_{y,i} e^{+jq_{z,i}d} = 0 \quad (43)$$

$$\sum_i \left(P_{x,i} + M_{y,i}/c_0\right)\left(\frac{1}{1 - e^{-j(q_{z,i} - k_0)d}}\right) = \frac{-j2ab\varepsilon_0 E_{inc,x}}{k_0} \quad (44)$$

where, in Eqs. (40) and (41) we have defined

$$\left(\alpha_E^{'xx}\right)^{-1} \equiv (\alpha_E^{xx})^{-1} - jk_0^3/6\pi \quad (45)$$

$$\left(\alpha_M^{'yy}\right)^{-1} \equiv \left(\alpha_E^{yy}\right)^{-1} - jk_0^3/6\pi, \quad (46)$$

respectively. It has been previously shown that the imaginary parts of $(\alpha_E^{xx})^{-1}$ and $(\alpha_M^{xx})^{-1}$ each contain the radiation damping term $+jk_0^3/6\pi$ [13, 23, 24]. In our definitions of $\left(\alpha_E^{'xx}\right)^{-1}$ and $\left(\alpha_M^{'yy}\right)^{-1}$ this radiation damping term is exactly canceled with its negative. Hence, $\alpha_E^{'xx}$ and $\alpha_M^{'yy}$ are recognized to be the polarizations computed without radiation damping.

Eqs. (40) and (41) will be used in the next section to determine the material wavenumbers, $q_{z,i}$. Eqs. (42) and (43) constitute the boundary conditions. Paralleling the interpretation by Mahan and Obermair of their results for all-dielectric crystals [2], these equations indicate that the electric- and magnetic-dipole moments both equal zero at a "fictitious" plane located at a distance $-d$ from the xy plane (corresponding to the fictitious planar index $n = -1$). Eq. (44) is a result of setting the group of terms proportional to $e^{-jk_0dn'}$ in Eqs. (38) and (39) equal to zero, and constitutes the discrete analog of the Ewald-Oseen extinction theorem for a magnetodielectric half-space. Essentially, the equation indicates that in discrete space each eigenmode produces a field traveling plane-to-plane in the $+z$ direction with wavenumber k_0 such that the sum total over all eigenmodes exactly cancels out the incident field. A similar expression was found by Philpott for the case of an all-dielectric crystal (see Eq. (4.11) in [4]; Philpott's expression is equivalent to our Eq. (44) in the special case of normal incidence and cubic geometry with $M_{y,i} = 0$.)

6. THE DISPERSION RELATION

Let us now turn our attention to Eqs. (40) and (41). These equations involve sums of terms proportional to $e^{-jq_{z,i}dn'}$ over index i. Because these equations hold true for all planar indices, $n' = 0, 1, 2, \ldots$, and because $q_{z,i}$ is independent of n', each term in the sum must separately equal zero:

$$P_{x,i}\left\{\tilde{C}_{0,\mathrm{SR}}^{\mathrm{TEM}_z,xx} + 2C_{1,\mathrm{SR}}^{\mathrm{TEM}_z,xx}\cos(q_{z,i}d) - \left(\alpha_E^{\prime xx}\right)^{-1}(ab)^{3/2} + \left(\frac{k_0(ab)^{1/2}}{2}\right)\left(\frac{\sin(k_0d)}{\cos(k_0d)-\cos(q_{z,i}d)}\right)\right\} + M_{y,i}\left\{\frac{1}{c_0}\left(\frac{k_0(ab)^{1/2}}{2}\right)\left(\frac{\sin(q_{z,i}d)}{\cos(k_0d)-\cos(q_{z,i}d)}\right)\right\} = 0 \quad (47)$$

$$P_{x,i}\left\{c_0\left(\frac{k_0(ab)^{1/2}}{2}\right)\left(\frac{\sin(q_{z,i}d)}{\cos(k_0d)-\cos(q_{z,i}d)}\right)\right\} + M_{y,i}\left\{\tilde{C}_{0,\mathrm{SR}}^{\mathrm{TEM}_z,yy} + 2C_{1,\mathrm{SR}}^{\mathrm{TEM}_z,yy}\cos(q_{z,i}d) - (ab)^{3/2}\left(a_M^{\prime yy}\right)^{-1} + \left(\frac{k_0(ab)^{1/2}}{2}\right)\frac{\sin(k_0d)}{\cos(k_0d)-\cos(q_{z,i}d)}\right\} = 0 \quad (48)$$

Eqs. (47) and (48) constitute a 2×2 set of linear equations for the unknown amplitudes $P_{x,i}$ and $M_{y,i}$. So that a nontrivial solution exists, we set the determinant of the matrix of the coefficient of variables equal to zero, which gives the dispersion relation for the structure. By performing this operation and simplifying, we arrive at the following dispersion relation written in the form of a cubic equation with variable $\cos(q_{z,i}d)$:

$$Q_3 w^3 + Q_2 w^2 + Q_1 w + Q_0 = 0; \quad w = \cos(q_{z,i}d) \tag{49}$$

where

$$Q_3 = 4C_{1,\mathrm{SR}}^{\mathrm{TEM}_z,yy} C_{1,\mathrm{SR}}^{\mathrm{TEM}_z,xx} \alpha_M^{'yy} \alpha_E^{'xx} \tag{50}$$

$$\begin{aligned} Q_2 &= 2\alpha_M^{'yy} C_{1,\mathrm{SR}}^{\mathrm{TEM}_z,yy} \left(\tilde{C}_{0,\mathrm{SR}}^{\mathrm{TEM}_z,xx} \alpha_E^{'xx} - (ab)^{3/2} \right) \\ &\quad + 2\alpha_E^{'xx} C_{1,\mathrm{SR}}^{\mathrm{TEM}_z,xx} \left(\tilde{C}_{0,\mathrm{SR}}^{\mathrm{TEM}_z,yy} \alpha_M^{'yy} - (ab)^{3/2} \right) \\ &\quad - 4\alpha_E^{'xx} \alpha_M^{'yy} C_{1,\mathrm{SR}}^{\mathrm{TEM}_z,yy} C_{1,\mathrm{SR}}^{\mathrm{TEM}_z,xx} \cos(k_0 d) \end{aligned} \tag{51}$$

$$\begin{aligned} Q_1 &= -\cos(k_0 d) 2 \left[\alpha_M^{'yy} C_{1,\mathrm{SR}}^{\mathrm{TEM}_z,yy} \left(\alpha_E^{'xx} \tilde{C}_{0,\mathrm{SR}}^{\mathrm{TEM}_z,xx} - (ab)^{3/2} \right) \right. \\ &\quad \left. + \alpha_E^{'xx} C_{1,\mathrm{SR}}^{\mathrm{TEM}_z,xx} \left(\alpha_M^{'yy} \tilde{C}_{0,\mathrm{SR}}^{\mathrm{TEM}_z,yy} - (ab)^{3/2} \right) \right] \\ &\quad + \left(\alpha_E^{'xx} \tilde{C}_{0,\mathrm{SR}}^{\mathrm{TEM}_z,xx} - (ab)^{3/2} \right) \left(\alpha_M^{'yy} \tilde{C}_{0,\mathrm{SR}}^{\mathrm{TEM}_z,yy} - (ab)^{3/2} \right) \\ &\quad - \sin(k_0 d) k_0 (ab)^{1/2} \left(C_{1,\mathrm{SR}}^{\mathrm{TEM}_z,xx} + C_{1,\mathrm{SR}}^{\mathrm{TEM}_z,yy} \right) \alpha_E^{'xx} \alpha_M^{'yy} \\ &\quad + k_0^2 \frac{(ab)}{4} \alpha_E^{'xx} \alpha_M^{'yy} \end{aligned} \tag{52}$$

$$\begin{aligned} Q_0 &= -\cos(k_0 d) \left(\alpha_E^{'xx} \tilde{C}_{0,\mathrm{SR}}^{\mathrm{TEM}_z,xx} - (ab)^{3/2} \right) \left(\alpha_M^{'yy} \tilde{C}_{0,\mathrm{SR}}^{\mathrm{TEM}_z,yy} - (ab)^{3/2} \right) \\ &\quad - \frac{1}{2} \sin(k_0 d) k_0 (ab)^{1/2} \left[\alpha_E^{'xx} \left(\alpha_M^{'yy} \tilde{C}_{0,\mathrm{SR}}^{\mathrm{TEM}_z,yy} - (ab)^{3/2} \right) \right. \\ &\quad \left. + \alpha_M^{'yy} \left(\alpha_E^{'xx} \tilde{C}_{0,\mathrm{SR}}^{\mathrm{TEM}_z,xx} - (ab)^{3/2} \right) \right] + \frac{k_0^2 (ab)}{4} \alpha_E^{'xx} \alpha_M^{'yy} \cos(k_0 d) \end{aligned} \tag{53}$$

By taking the inverse cosine of the roots of Eq. (49), the eigenvalues $q_{z,i}$ are found within a plus or minus sign. For the lossy case we choose the sign of $q_{z,i}$ corresponding to a negative imaginary component ($\mathrm{Im}[q_{z,i}] < 0$). In this manner, the eigenmodes decay along the z-axis. For the lossless case, we choose the sign corresponding to positive energy transfer to the $z \geq 0$ half-space, such that $\partial q_{z,i}/\partial \omega > 0$. For practical numerical calculations of lossless structures, the sign can

also be determined by first introducing a very small loss term into the system and choosing the appropriate sign that gives a negative imaginary part. This can be considered as the numerical counterpart to the principle of limiting absorption. We note that our solution is not unique in the sense that one can always add the real term $2\pi n_t/d$, where n_t is an arbitrary integer, to $q_{z,i}$ and arrive at the same final answer to the scattering problem. This is because the term $q_{z,i}$ appears solely in our formulas as an argument (multiplied by d) to a complex exponential function (i.e., $e^{-jq_{z,i}d}$), and $e^{-jq_{z,i}d} = e^{-j(q_{z,i}+2\pi n_t/d)d}$.

The dispersion relation given by Eq. (49) has precisely three roots because we included only nearest-neighbor near-field interactions in the analysis. In general, for magnetodielectric crystals in the case of normal incidence, including L near-field interactions results in a polynomial of degree $1 + 2L$. This is in contrast to an all-dielectric or all-magnetic structure in which the number of roots is $1 + L$ [2].

Recently, Simovski et al. derived the dispersion relation, in two alternative equivalent forms, for a magnetodielectric crystal with simultaneous electric and magnetic dipole moments [15, 16] (akin to the structure we are considering here). However, in these works the authors ignore all near-field interactions between neighboring planes. While this is adequate for investigating bulk properties, we include nearest-neighbor interactions, because, as Berman demonstrated for the all-dielectric case [19], such near-field interactions are crucial for accurately modeling and investigating realistic surface effects.

7. THE REFLECTION COEFFICIENT OF A METAMATERIAL HALF-SPACE

After the eigenvalues are determined using the dispersion relation given by Eq. (49), the magnetic-to-electric amplitude ratio for each mode, denoted $B_{yx,i}^{\mathrm{TEM}_z} \equiv M_{y,i}/(c_0 P_{x,i})$ can be found using Eq. (47) (or equivalently Eq. (48)):

$$B_{yx,i}^{\mathrm{TEM}_z} \equiv \frac{M_{y,i}}{c_0 P_{x,i}} = \frac{\tilde{C}_{0,\mathrm{SR}}^{\mathrm{TEM}_z,xx} + 2C_{1,\mathrm{SR}}^{\mathrm{TEM}_z,xx}\cos(q_{z,i}d) - \left(\alpha_E'^{xx}\right)^{-1}(ab)^{3/2} + \frac{(k_0/2)(ab)^{1/2}\sin(k_0 d)}{\cos(k_0 d)-\cos(q_{z,i}d)}}{\left(\frac{k_0(ab)^{1/2}}{2}\right)\left(\frac{\sin(q_{z,i}d)}{\cos(q_{z,i}d)-\cos(k_0 d)}\right)}$$

$$= \frac{\left(\frac{k_0(ab)^{1/2}}{2}\right)\left(\frac{\sin(q_{z,i}d))}{\cos(q_{z,i}d)-\cos(k_0d)}\right)}{\tilde{C}^{\mathrm{TEM}_z,yy}_{0,\mathrm{SR}}+C^{\mathrm{TEM}_z,yy}_{1,\mathrm{SR}}\cos(q_{z,i}d)-\left(\alpha'^{yy}_M\right)^{-1}(ab)^{3/2}+\frac{(k_0/2)(ab)^{1/2}\sin(k_0d)}{\cos(k_0d)-\cos(q_{z,i}d)}} \tag{54}$$

Given the amplitude ratios $B^{\mathrm{TEM}_z}_{yx,i}$; $(i = 1, 2, 3)$ we can now rewrite Eqs. (42)–(44) as a 3×3 set of linear equations that can be used to solve for the three unknown amplitudes, $P_{x,i}$; $(i = 1, 2, 3)$

$$\begin{bmatrix} e^{+jq_{z,1}d} & e^{+jq_{z,2}d} & e^{+jq_{z,3}d} \\ B^{\mathrm{TEM}_z}_{yx,1}e^{+jq_{z,1}d} & B^{\mathrm{TEM}_z}_{yx,2}e^{+jq_{z,2}d} & B^{\mathrm{TEM}_z}_{yx,3}e^{+jq_{z,3}d} \\ \frac{1+B^{\mathrm{TEM}_z}_{yx,1}}{1-e^{-j(q_{z,1}-k_0)d}} & \frac{1+B^{\mathrm{TEM}_z}_{yx,2}}{1-e^{-j(q_{z,2}-k_0)d}} & \frac{1+B^{\mathrm{TEM}_z}_{yx,3}}{1-e^{-j(q_{z,3}-k_0)d}} \end{bmatrix} \begin{bmatrix} P_{x,1} \\ P_{x,2} \\ P_{x,3} \end{bmatrix}$$

$$= \begin{bmatrix} 0 \\ 0 \\ \tilde{E}_{inc,x} \end{bmatrix}, \tag{55}$$

where we have defined $\tilde{E}_{inc,x} \equiv -j2ab\varepsilon_0 E_{inc,x}/k_0$. The solutions of Eq. (55) are:

$$P_{x,1} = \frac{\tilde{E}_{inc,x}\left(B^{\mathrm{TEM}_z}_{yx,3} - B^{\mathrm{TEM}_z}_{yx,2}\right)e^{-jq_{z,1}d}}{\Delta_D} \tag{56}$$

$$P_{x,2} = \frac{\tilde{E}_{inc,x}\left(B^{\mathrm{TEM}_z}_{yx,1} - B^{\mathrm{TEM}_z}_{yx,3}\right)e^{-jq_{z,2}d}}{\Delta_D} \tag{57}$$

$$P_{x,3} = \frac{\tilde{E}_{inc,x}\left(B^{\mathrm{TEM}_z}_{yx,2} - B^{\mathrm{TEM}_z}_{yx,1}\right)e^{-jq_{z,3}d}}{\Delta_D} \tag{58}$$

where:

$$\Delta_D \equiv \frac{\left(B^{\mathrm{TEM}_z}_{yx,1}+1\right)\left(B^{\mathrm{TEM}_z}_{yx,2}-B^{\mathrm{TEM}_z}_{yx,3}\right)}{e^{jk_0d}-e^{jq_{z,1}d}} + \frac{\left(B^{\mathrm{TEM}_z}_{yx,2}+1\right)\left(B^{\mathrm{TEM}_z}_{yx,3}-B^{\mathrm{TEM}_z}_{yx,1}\right)}{e^{jk_0d}-e^{jq_{z,2}d}} + \frac{\left(B^{\mathrm{TEM}_z}_{yx,3}+1\right)\left(B^{\mathrm{TEM}_z}_{yx,1}-B^{\mathrm{TEM}_z}_{yx,2}\right)}{e^{jk_0d}-e^{jq_{z,3}d}} \tag{59}$$

The electric dipole distribution $\{p^{(x)}_n\}$ is found by substituting $P_{x,i}$; $(i = 1, 2, 3)$ given by Eqs. (56)–(58) into Eq. (26). The

magnetic dipole distribution $\{m_n^{(y)}\}$ is found by substituting $M_{y,i} = c_0 B_{yx,i}^{\mathrm{TEM}_z} P_{x,i}$; $(i = 1, 2, 3)$, as determined using Eqs. (54), (56)–(58), into Eq. (27).

The total scattered electric field in the air region ($z < 0$) is a superposition of a reflected plane wave $\boldsymbol{E}_r = \hat{\boldsymbol{a}}_x S_{11}^{\mathrm{half}} E_{inc,x} e^{-jk_0|z|}$ and a combination of scattered evanescent waves produced by the lattice, all of which decay rapidly to zero with increasing distance normal from the surface. For observation points a sufficient distance away from the surface (generally three lattice periods in the normal direction is adequate for a cubic lattice), the evanescent fields are negligible and the total scattered field equals that of the reflected plane wave.

The plane wave component of the electric field produced by a single lattice of dipoles in plane $z = dn'$ with electric dipole moment distribution $\boldsymbol{p}_{n'} = \boldsymbol{a}_x p_{n'}^{(x)}$ and magnetic dipole moment distribution $\boldsymbol{m}_{n'} = \boldsymbol{a}_y m_{n'}^{(y)}$ is given by $\boldsymbol{E}_{n'}^{\mathrm{scat}}(z) = \boldsymbol{a}_x (E_{n'}^p e^{-jk_0|z-dn'|} \pm E_{n'}^m e^{-jk_0|z-dn'|})$ where $E_{n'}^p = -jp_{n'}^{(x)} \omega\eta_0/(2ab)$, $E_{n'}^m = -jm_{n'}^{(y)} \omega\mu_0/(2ab)$, and the sign $\pm$ corresponds to half spaces $z > dn'$ and $z < dn'$, respectively. Note that $\boldsymbol{E}_{n'}^{\mathrm{scat}}(z)$ describes the plane wave produced by an equivalent current sheet carrying electric current density $\boldsymbol{J}_s = \boldsymbol{a}_x j\omega p_{n'}^{(x)}/(ab)$ and magnetic current density $\boldsymbol{M}_s = \boldsymbol{a}_x j\omega m_{n'}^{(y)}/(ab)$. Using this expression, we find the reflection coefficient for the half-space S_{11}^{half} by summing the electric field amplitudes (normalized by $E_{inc,x}$) produced by each array of discrete elements evaluated at the reference plane $z = 0$:

$$\begin{aligned} S_{11}^{\mathrm{half}} &= \frac{1}{E_{inc,x}} \sum_{n=0}^{\infty} \boldsymbol{E}_n^{\mathrm{scat}}(z=0) \\ &= \frac{k_0}{jE_{inc,x}\varepsilon_0 2ab} \sum_{n=0}^{\infty} \left(p_n^{(x)} - \frac{m_n^{(y)}}{c_0} \right) e^{-jk_0 dn} \\ &= \frac{k_0}{jE_{inc,x}\varepsilon_0 2ab} \sum_{i=1}^{3} \sum_{n=0}^{\infty} P_{x,i} e^{-j(q_{z,i}+k_0)dn} \left(1 - B_{yx,i}^{\mathrm{TEM}_z} \right) \\ &= \frac{-1}{\tilde{E}_{inc,x}} \sum_{i=1}^{3} P_{x,i} \frac{1 - B_{yx,i}^{\mathrm{TEM}_z}}{1 - e^{-j(q_{z,i}+k_0)d}} \end{aligned} \tag{60}$$

where we invoked the principle of limiting absorption to ensure convergence of the geometric series. Substituting the amplitudes $P_{x,i}$; $(i = 1, 2, 3)$ given by Eqs. (56)–(58) into Eq. (60) and simplifying

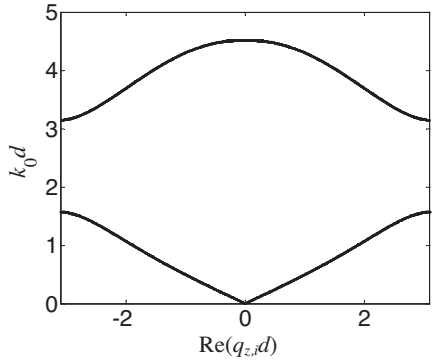

Figure 3. Dispersion diagram showing the first two pass bands for a cubic lattice of nonmagnetic particles with polarizability densities, $\alpha'_E N_v = \pi/2$ and $\alpha'_M N_v = 0$ (substituting these values into Eqs. (63) and (64) results in the following corresponding effective medium parameters: $\varepsilon^{\mathrm{CM}}_{r,eff} = 4.297$ and $\mu^{\mathrm{CM}}_{r,eff} = 1$).

yields our desired result:

$$S_{11}^{\mathrm{half}} = \frac{\Delta_N}{\Delta_D} \tag{61}$$

where Δ_D is defined by Eq. (59) and Δ_N is defined as:

$$\Delta_N \equiv \frac{\left(B_{yx,1}^{\mathrm{TEM}_z} - 1\right)\left(B_{yx,2}^{\mathrm{TEM}_z} - B_{yx,3}^{\mathrm{TEM}_z}\right)}{e^{-jk_0 d} - e^{jq_{z,1}d}} + \frac{\left(B_{yx,2}^{\mathrm{TEM}_z} - 1\right)\left(B_{yx,3}^{\mathrm{TEM}_z} - B_{yx,1}^{\mathrm{TEM}_z}\right)}{e^{-jk_0 d} - e^{jq_{z,2}d}} + \frac{\left(B_{yx,3}^{\mathrm{TEM}_z} - 1\right)\left(B_{yx,1}^{\mathrm{TEM}_z} - B_{yx,2}^{\mathrm{TEM}_z}\right)}{e^{-jk_0 d} - e^{jq_{z,3}d}} \tag{62}$$

8. PROPERTIES OF THE DISPERSION RELATION

In this section, the dispersion relation given by Eq. (49) is solved numerically for a cubic lattice ($a = b = d$) of isotropic particles with electric and magnetic polarizabilities denoted $\alpha'_E \equiv \alpha'^{xx}_E = \alpha'^{yy}_E = \alpha'^{zz}_E$ and $\alpha'_M \equiv \alpha'^{xx}_M = \alpha'^{yy}_M = \alpha'^{zz}_M$, respectively. In Fig. 3 the dispersion diagram is plotted for a dielectric crystal with parameters, $\alpha'_E N_v = \pi/2$ and $\alpha'_M N_v = 0$, where $N_v = d^{-3}$ is the volume density of dipoles; these parameters correspond to the quasi-static polarizabilities of a densely packed lattice of conducting spheres (recall that the static electric and

magnetic polarizabilities for a conducting sphere with volume V_{vol} are $\alpha_E = 3V_{vol}$ and $\alpha_M = 0$, respectively [25]). From the figure, we see that the first passband (between $k_0 d = 0$ and $k_0 d = 1.6$) corresponds to a single purely real solution for the propagation constant, while the other two solutions are purely imaginary. In the first stopband (between $k_0 d = 1.6$ and $k_0 d = 3.14$) all solutions for the propagation constant are purely imaginary. In the second passband (between $k_0 d = 3.14$ and $k_0 d = 4.5$), we have a single purely real solution which exhibits negative dispersion; meaning the phase velocity $v_p = \omega/q_z$ is opposite in sign to the group velocity $v_g = \partial\omega/\partial q_z$. In general, as $k_0 d$ increases beyond what is shown, the dispersive behavior continues to alternate between bands and gaps as demonstrated in references [12, 26], which is characteristic of a photonic bandgap crystal.

Within the framework of the quasi-static approximation, the Clausius-Mossotti approximation relates the effective relative permittivity $\varepsilon_{r,eff}$ and effective relative permeability $\mu_{r,eff}$ to the electric and magnetic polarizabilities of the particles, respectively. For a cubic lattice of isotropic particles, the Clausius-Mossotti relations take the form:

$$\varepsilon_{r,eff}^{\mathrm{CM}} = \frac{1 + (2/3)N_v \alpha'_E}{1 - (1/3)N_v \alpha'_E} \tag{63}$$

$$\mu_{r,eff}^{\mathrm{CM}} = \frac{1 + (2/3)N_v \alpha'_M}{1 - (1/3)N_v \alpha'_M} \tag{64}$$

We should keep in mind that Eqs. (63) and (64) follow from the approximations inherent to the Clausius-Mossotti approach and may not represent the "true" homogenized parameters; such approximations include operation in the long-wavelength regime ($k_0 a \ll 1$) with negligible spatial dispersion. Hence, the theory only accounts for purely "bulk" properties sufficiently far away from discontinuities and surfaces. To remind us of this fact, we include the superscript "CM" in the notation in Eqs. (63) and (64). In the homogenous media approximation (HMA), the electrical length of a single unit cell $q_z d$ is simply given by the light line in the effective medium, $q_z d = n_{eff}^{\mathrm{CM}} k_0 d$, where n_{eff}^{CM} is the effective index of refraction determined within the Clausius-Mossotti formulism, i.e., $n_{eff}^{\mathrm{CM}} = \sqrt{\varepsilon_{r,eff}^{\mathrm{CM}} \mu_{r,eff}^{\mathrm{CM}}}$ where $\varepsilon_{r,eff}^{\mathrm{CM}}$ and $\mu_{r,eff}^{\mathrm{CM}}$ are calculated from Eqs. (63) and (64).

In Fig. 4 we compare the dispersion curves for a cubic structure for three different sets of polarizabilities; for each set we choose the parameters $\alpha'_E N_v$ and $\alpha'_M N_v$ such that the corresponding index of

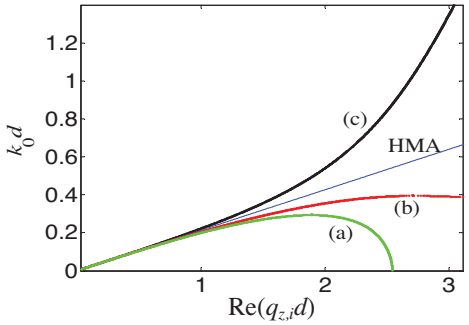

Figure 4. Dispersion diagram for a cubic lattice of particles with polarizability densities, $\alpha'_E N_v$ and $\alpha'_M N_v$, chosen such that the corresponding index of refraction is $n_{eff}^{\mathrm{CM}} = \sqrt{\varepsilon_{r,eff}^{\mathrm{CM}} \mu_{r,eff}^{\mathrm{CM}}} = \sqrt{22}$ where $\varepsilon_{r,eff}^{\mathrm{CM}}$ and $\mu_{r,eff}^{\mathrm{CM}}$ are calculated using Eqs. (63) and (64), respectively: (a) $\alpha'_E N_v = 2.625$ and $\alpha'_M N_v = 0$ ($\varepsilon_{r,eff}^{\mathrm{CM}} = 22$ and $\mu_{r,eff}^{\mathrm{CM}} = 1$), (b) $\alpha'_E N_v = 2.571$ and $\alpha'_M N_v = 0.15$ ($\varepsilon_{r,eff}^{\mathrm{CM}} = 19$ and $\mu_{r,eff}^{\mathrm{CM}} = 1.158$), and (c) $\alpha'_E N_v = 1.165$ and $\alpha'_M N_v = 1.165$ ($\varepsilon_{r,eff}^{\mathrm{CM}} = \sqrt{22}$ and $\mu_{r,eff}^{\mathrm{CM}} = \sqrt{22}$). For reference we also plot the light line in the effective medium $q_z d = n_{eff}^{\mathrm{CM}} k_0 d$ as determined by the homogenous media approximation (HMA).

refraction, $n_{eff}^{\mathrm{CM}} = \sqrt{\varepsilon_{r,eff}^{\mathrm{CM}} \mu_{r,eff}^{\mathrm{CM}}} = \sqrt{22}$. The three dispersion curves are labeled (a)–(c) in the plot and the corresponding values of $\alpha'_E N_v$ and $\alpha'_M N_v$ are given in the figure caption. The light line in the effective medium, $q_z d = n_{eff}^{\mathrm{CM}} k_0 d$, as determined by the HMA is also plotted for reference. The most striking feature of this plot is the behavior of case (a), which corresponds to parameters $\alpha'_E N_v = 2.625$ and $\alpha'_M N_v = 0$ ($\varepsilon_{r,eff}^{\mathrm{CM}} = 22$ and $\mu_{r,eff}^{\mathrm{CM}} = 1$). From the plot of the dispersion curve (a), we see that there exist two purely real solutions for the propagation constant at all frequencies below the first bandgap. Even in the static limit $k_0 d \to 0$ we have two solutions, $q_z d = 0$ and $q_z d = 2.54$. It follows, that in the static limit, the lattice supports a steady, periodic, electric dipole moment distribution with wavelength $\lambda_1 = 2\pi/q_z = 2.47d$. In the context of a general one-dimensional periodic structure, the possibility of having two solutions in the static limit has been pointed out and discussed by Brillouin (e.g., see Sec. 8 and Sec. 10 in [27]).

To help explain this behavior, we find that, in the long-wavelength

limit, the solutions to the dispersion relation Eq. (49) are:

$$q_{z,1}d = \pm k_0 d$$

$$\left[1+\frac{-\frac{(ab)^{1/2}}{d}\left[\begin{array}{l}\alpha_E^{'xx}\alpha_M^{'yy}\left(2C_{1,\mathrm{SR}}^{\mathrm{TEM}_z,xx}+2C_{1,\mathrm{SR}}^{\mathrm{TEM}_z,yy}+\right.\\ \left.\tilde{C}_{0,\mathrm{SR}}^{\mathrm{TEM}_z,xx}+\tilde{C}_{0,\mathrm{SR}}^{\mathrm{TEM}_z,yy}-\frac{(ab)^{1/2}}{d}\right)\\ -\left(\alpha_E^{'xx}+\alpha_M^{'yy}\right)(ab)^{3/2}\end{array}\right]}{\left[\begin{array}{l}\left(\alpha_E^{'xx}\left(\tilde{C}_{0,\mathrm{SR}}^{\mathrm{TEM}_z,xx}+2C_{1,\mathrm{SR}}^{\mathrm{TEM}_z,xx}\right)-(ab)^{3/2}\right)\\ \times\left(\alpha_M^{'yy}\left(\tilde{C}_{0,\mathrm{SR}}^{\mathrm{TEM}_z,yy}+2C_{1,\mathrm{SR}}^{\mathrm{TEM}_z,yy}\right)-(ab)^{3/2}\right)\end{array}\right]}\right]^{\frac{1}{2}} \tag{65}$$

$$q_{z,2}d = \pm\arccos\left(\frac{\tilde{C}_{0,\mathrm{SR}}^{\mathrm{TEM}_z,xx}\alpha_E^{'xx}-(ab)^{3/2}}{2C_{1,\mathrm{SR}}^{\mathrm{TEM}_z,xx}\alpha_E^{'xx}}\right) \tag{66}$$

$$q_{z,3}d = \pm\arccos\left(\frac{\tilde{C}_{0,\mathrm{SR}}^{\mathrm{TEM}_z,yy}\alpha_M^{'yy}-(ab)^{3/2}}{2C_{1,\mathrm{SR}}^{\mathrm{TEM}_z,yy}\alpha_M^{'yy}}\right). \tag{67}$$

The solution specified by Eq. (65) corresponds to the "ordinary" propagation constant as calculated using the conventional HMA for a rectangular lattice, while the solutions specified by Eqs. (66) and (67) correspond to "extraordinary" modes that are excited at the surface of the air-metamaterial interface. To have more than one purely real solution for the propagation constant (such that at least one of the two extraordinary modes is non-decaying), the particles must be lossless (i.e., $\mathrm{Im}(\alpha_E^{'xx}) = \mathrm{Im}(\alpha_M^{'yy}) = 0$), and the argument of the arccos function in Eq. (66) and/or Eq. (67) must be purely real and less than or equal to one in magnitude, i.e.,

$$\left|\frac{\tilde{C}_{0,\mathrm{SR}}^{\mathrm{TEM}_z,xx}\alpha_E^{'xx}-(ab)^{3/2}}{2C_{1,\mathrm{SR}}^{\mathrm{TEM}_z,xx}\alpha_E^{'xx}}\right| \leq 1 \tag{68}$$

$$\left|\frac{\tilde{C}_{0,\mathrm{SR}}^{\mathrm{TEM}_z,yy}\alpha_M^{'yy}-(ab)^{3/2}}{2C_{1,\mathrm{SR}}^{\mathrm{TEM}_z,yy}\alpha_M^{'yy}}\right| \leq 1 \tag{69}$$

For the special case of a cubic lattice, Eqs. (68) and (69) simplify to:

$$\frac{1}{\tilde{C}_{0,\mathrm{SR}}^{\mathrm{TEM}_z,xx}+2C_{1,\mathrm{SR}}^{\mathrm{TEM}_z,xx}} \leq \alpha_E^{'xx}N_v \leq \frac{1}{\tilde{C}_{0,\mathrm{SR}}^{\mathrm{TEM}_z,xx}-2C_{1,\mathrm{SR}}^{\mathrm{TEM}_z,xx}}, \tag{70}$$

$$\frac{1}{\tilde{C}_{0,\mathrm{SR}}^{\mathrm{TEM}_z,yy}+2C_{1,\mathrm{SR}}^{\mathrm{TEM}_z,yy}} \leq \alpha_M^{'yy}N_v \leq \frac{1}{\tilde{C}_{0,\mathrm{SR}}^{\mathrm{TEM}_z,yy}-2C_{1,\mathrm{SR}}^{\mathrm{TEM}_z,yy}}. \tag{71}$$

For a cubic lattice in the static limit, the numerical values of the first two planar interaction constants are $\tilde{C}_{0,\mathrm{SR}}^{\mathrm{TEM}_z,xx} = \tilde{C}_{0,\mathrm{SR}}^{\mathrm{TEM}_z,yy} = 0.3594$ and $C_{1,\mathrm{SR}}^{\mathrm{TEM}_z,xx} = C_{1,\mathrm{SR}}^{\mathrm{TEM}_z,yy} = -0.0130$. By substituting these values into Eqs. (70) and (71), and in turn substituting $\alpha_E^{'xx}$ and $\alpha_M^{'yy}$ into the Clausius-Mossotti Eqs. (63) and (64), we find that there will be more than one purely real solution to the propagation constant if the corresponding effective permittivity and/or permeability are numerically greater than or equal to 20.2 (i.e., $\varepsilon_{r,eff}^{\mathrm{CM}} \geq 20.2$ and/or $\mu_{r,eff}^{\mathrm{CM}} \geq 20.2$). In [28], Kar and Bagchi solved for the electric dipole moment distribution in the quasi-static limit near the surface of a cubic electric-dipole lattice using a simple matrix inversion technique. In this work, they found that the inversion procedure breaks down for a range of electric polarizabilities equivalent to that specified by our Eq. (70) in which the system supports "spontaneous polarization modes". Mochan and Barrera have also noted special cases in which the polarization in dielectric crystals exhibits higher-order oscillations which do not decay [29].

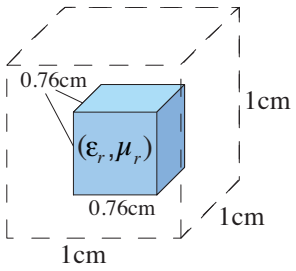

Figure 5. Unit cell composed of a magnetodielectric cube centered in a free-space cubical region.

Commonly, only near resonances do particles exhibit polarizabilities for which Eqs. (68) and (69) hold. Consider a metamaterial composed of a cubic lattice of magnetodielectric cubical particles in which the unit cell is shown in Fig. 5. The lattice period $d = 1\,\mathrm{cm}$ and the particle edge length is 0.76 cm. As a hypothetical material, we choose the relative permittivity ε_r and relative permeability μ_r of the magnetodielectric cube to be $\mathrm{Re}(\varepsilon_r) = \mathrm{Re}(\mu_r) = 500$ with loss tangents of $\tan\delta_E = \tan\delta_M = 5 \times 10^{-4}$ (these parameters describe the cube and are not to be confused with the effective parameters of the composite as a whole). With these parameters, the particle undergoes its first resonance around 94.06 MHz ($k_0 d = 0.0197$). A single lattice of such particles were simulated using Ansoft HFSS (a commercially available

finite-element based electromagnetic solver) and the polarizabilities extracted using the method presented in [23]. By symmetry of the problem, the electric and magnetic polarizabilities are numerically equal. Fig. 6 shows a plot of the real part of the extracted electric polarizability density $\alpha'_E N_v$ and the real part of the corresponding effective permittivity $\varepsilon^{\mathrm{CM}}_{r,eff}$ calculated using Eq. (63). As the curve $\mathrm{Re}(\alpha'_E N_v)$ goes through resonance, it intersects the line $\mathrm{Re}(\alpha'_E N_v) = 3$. This is the point at which the denominator of Eq. (63) approaches zero and the effective permittivity reaches its maximum. As $\mathrm{Re}(\alpha'_E N_v)$ increases beyond this point, $\mathrm{Re}(\varepsilon^{\mathrm{CM}}_{r,eff})$ flips sign and becomes negative.

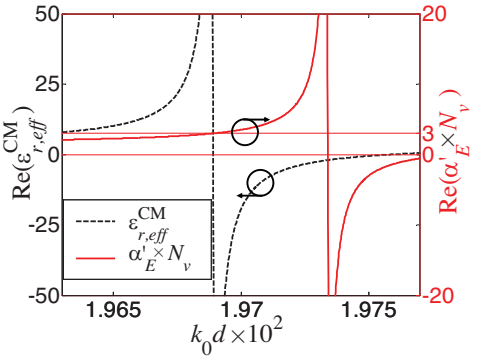

Figure 6. Real part of the electric polarizability density and effective permittivity vs. $k_0 d$ for a metamaterial composite with the unit cell shown in Fig. 5 for $\mathrm{Re}(\varepsilon_r) = \mathrm{Re}(\mu_r) = 500$ and $\tan\delta_E = \tan\delta_M = 5 \times 10^{-4}$. Because the particles are matched, a corresponding plot of the magnetic polarizability density and the effective permeability vs. $k_0 d$ is numerically equivalent to the plot shown.

Fig. 7 presents the dispersion diagram for the structure in the previous example as determined using both the present method and the Ansoft HFSS eigensolver; the latter being included as an independent check for comparison. Because of the small loss tangent of the magnetodielectric cube, there exist no purely real solutions for the propagation constant, and the results shown are for eigenmodes with slowest decay. Both techniques exhibit good agreement and both demonstrate a small frequency band near resonance in which there exists simultaneous propagating modes. In particular, the HFSS eigensolver shows that the three simultaneous modes propagate within the frequency band $k_0 d = 0.019674$ to $k_0 d = 0.019679$ (0.025% bandwidth).

Consider again a metamaterial in which the geometry of the unit

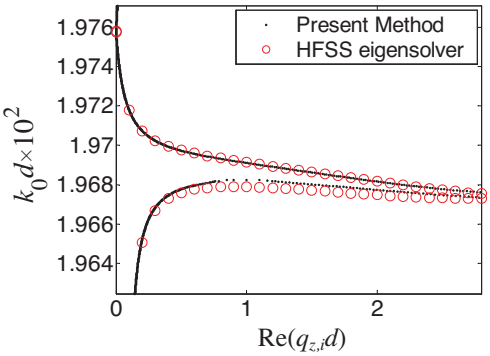

Figure 7. Dispersion diagram for a metamaterial composed of a cubic lattice of magnetodielectric cubes in which the unit cell is shown in Fig. 5 and $\mathrm{Re}(\varepsilon_r) = \mathrm{Re}(\mu_r) = 500$ and $\tan\delta_E = \tan\delta_M = 5 \times 10^{-4}$.

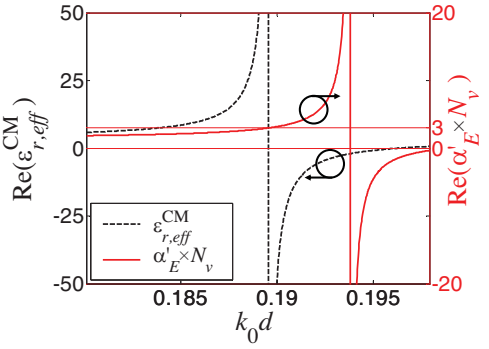

Figure 8. Real part of the electric polarizability density and effective permittivity vs. $k_0 d$ for a metamaterial composite with the unit cell shown in Fig. 5 for $\mathrm{Re}(\varepsilon_r) = \mathrm{Re}(\mu_r) = 50$ and $\tan\delta_E = \tan\delta_M = 5 \times 10^{-4}$. Because the particles are matched, a corresponding plot of the magnetic polarizability density and the effective permeability vs. $k_0 d$ is numerically equivalent to the plot shown.

cell is shown in Fig. 5. Let us choose the relative permittivity ε_r and the relative permeability μ_r of the magnetodielectric cube to each be ten times smaller than the corresponding parameters in the previous example, i.e., $\mathrm{Re}(\varepsilon_r) = \mathrm{Re}(\mu_r) = 50$ with a loss tangent of $\tan\delta_E = \tan\delta_M = 5 \times 10^{-4}$. With these parameters, the particle undergoes its first resonance around 0.907 GHz ($k_0 d = 0.19$). Fig. 8 shows a plot of the real part of the extracted electric polarizability density $\alpha'_E N_v$ and the corresponding effective permittivity $\varepsilon^{\mathrm{CM}}_{r,eff}$ calculated

using Eq. (63). Fig. 8 presents the dispersion diagram for the structure determined using both the present method and the HFSS eigensolver. Both methods exhibit good agreement and, as opposed to the previous example, both demonstrate no frequency bands in which multiple modes exist simultaneously. At first glance, this may seem to contradict the previous findings in which we stated that simultaneous propagating modes exist if the effective permittivity and/or permeability are numerically greater than or equal to 20.2, because from Fig. 8, we clearly see that this condition is satisfied near resonance. However, this special condition only applies to the first passband. In this example, the resonant frequency is roughly ten times higher than in the previous example, and, consequently, near resonance the composite operates in a higher passband in which only one mode propagates.

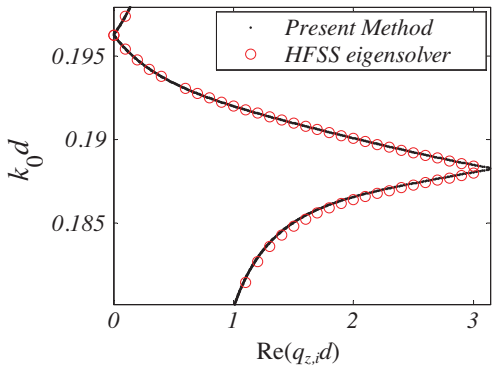

Figure 9. Dispersion diagram for a metamaterial composed of a cubic lattice of magnetodielectric cubes in which the unit cell is shown in Fig. 5, $\mathrm{Re}(\varepsilon_r) = \mathrm{Re}(\mu_r) = 50$ and $\tan\delta_E = \tan\delta_M = 5 \times 10^{-4}$.

9. DIPOLE MOMENT DISTRIBUTION NEAR THE BOUNDARY OF FREE-SPACE AND A SEMI-INFINITE METAMATERIAL

Let us now investigate how the polarization distribution varies from plane-to-plane near the surface of a semi-infinite metamaterial. Fig. 10 displays the magnitude of the dipole moment distribution $|p_n^{(x)}|$ at planes $n = 0, 1, \ldots, 9$ calculated using the equations presented in Sec. 8 for three different sets of parameters involving non-magnetic particles: (a) $\alpha'_E N_v = 1.71$, $\alpha'_M N_v = 0$ ($\varepsilon^{\mathrm{CM}}_{r,eff} = 5$, $\mu^{\mathrm{CM}}_{r,eff} = 1$), (b) $\alpha'_E N_v = 2.47$, $\alpha'_M N_v = 0$ ($\varepsilon^{\mathrm{CM}}_{r,eff} = 15$, $\mu^{\mathrm{CM}}_{r,eff} = 1$), and (c)

$\alpha'_E N_v = 2.57$, $\alpha'_M N_v = 0$ ($\varepsilon^{\mathrm{CM}}_{r,eff} = 19$, $\mu^{\mathrm{CM}}_{r,eff} = 1$). In this display, the magnitudes for each case are normalized to that of the "bulk" value taken here to be the magnitude at plane $n = 9$. In the calculations, the free-space electric length per unit cell is $k_0 d = 0.01$ and the lattice is cubic ($a = b = d$). We see from Fig. 10 that the polarization undergoes near-surface oscillations before settling into its bulk behavior. The appearance of such "wiggles" in the polarization near the boundaries of electric-dipolar slabs was discussed in some detail by Poppe et al. [30] and later by Berman [19]. In the context of the eigenmode approach, these wiggles are explained by the presence of an extraordinary mode that is excited at the surface in addition to the ordinary propagating mode. We emphasize that for a purely non-magnetic structure, only one extraordinary mode is excited if the nearest-neighbor approximation is made, as originally established by Mahan and Obermair [2]. For the three cases considered in Fig. 10 the extraordinary mode is evanescent. Its decay length is dependent on the value of the electric polarizability density $\alpha'_E N_v$; specifically, as the size of $\alpha'_E N_v$ is enlarged, the decay length increases accordingly. This is consistent with the behavior of the extraordinary mode's wavenumber as determined using Eqs. (66) and agrees with the findings of Gadomskii and Sukhov [31].

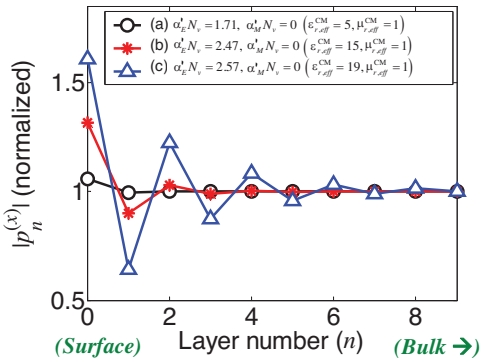

Figure 10. Polarization variation near the boundary of a non-magnetic metamaterial half-space at planes $n = 0, 1, \ldots,$ and 9 for three different cases involving evanescent extra-ordinary modes. $k_0 d = 0.01$.

For case (c) in Fig. 10, corresponding to the polarizability densities, $\alpha'_E N_v = 2.57$ and $\alpha'_M N_v = 0$ ($\varepsilon^{\mathrm{CM}}_{r,eff} = 19$ and $\mu^{\mathrm{CM}}_{r,eff} = 1$), the near-surface oscillations decay to zero approximately within the first ten lattice planes. If we increase $\alpha'_E N_v$, then the decay length increases in kind, until the perturbation eventually extends

throughout the entire structure. At this point, the structure supports a propagating extraordinary mode. This occurs when $\alpha'_E N_v$ satisfies the inequality given by Eq. (70), which is equivalent to the condition $\varepsilon^{\mathrm{CM}}_{r,eff} \geq 20.2$. Fig. 11 displays the magnitude of the dipole polarization $|p_n^{(x)}|$ calculated near the boundary for such a case; here we choose the polarizability densities to be $\alpha'_E N_v = 2.63$ and $\alpha'_M N_v = 0$ ($\varepsilon^{\mathrm{CM}}_{r,eff} = 22$ and $\mu^{\mathrm{CM}}_{r,eff} = 1$). From the figure we see that the propagating extraordinary mode has the effect of modulating the amplitude of the ordinary mode in the discretized spatial domain.

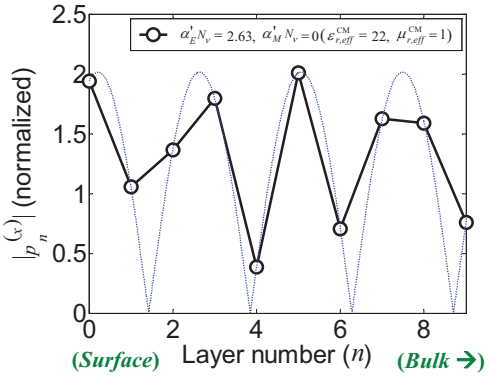

Figure 11. Polarization variation near the boundary of a non-magnetic metamaterial half-space at planes $n = 0, 1, \ldots,$ and 9 for a case involving a propagating extra-ordinary mode. The polarization is normalized to the magnitude at plane $n = 10$, $k_0 d = 0.01$.

Fig. 12 displays the magnitude of the dipole polarization $|p_n^{(x)}|$ calculated at the planes $n = 0, 1, \ldots, 9$ for three different sets of double-negative parameters ($\varepsilon^{\mathrm{CM}}_{r,eff} < 0$ and $\mu^{\mathrm{CM}}_{r,eff} < 1$): (a) $\alpha'_E N_v = 6$, $\alpha'_M N_v = -6$ ($\varepsilon^{\mathrm{CM}}_{r,eff} = -5$ and $\mu^{\mathrm{CM}}_{r,eff} = -1$), (b) $\alpha'_E N_v = 3.7$, $\alpha'_M N_v = -6$ ($\varepsilon^{\mathrm{CM}}_{r,eff} = -15$, $\mu^{\mathrm{CM}}_{r,eff} = -1$), and (c) $\alpha'_E N_v = 3.53$, $\alpha'_M N_v = -6$ ($\varepsilon^{\mathrm{CM}}_{r,eff} = -19$, $\mu^{\mathrm{CM}}_{r,eff} = -1$). As in the previous examples, the free-space electric length per unit cell is $k_0 d = 0.01$ and the lattice is cubic ($a = b = d$). For all three cases, the polarization variation settles into its bulk behavior within three or four lattice planes from the boundary and, as opposed to the behavior in the previous examples, the damping does not oscillate. This behavior is reminiscent of the response of an over-damped system.

In passing, we point out that the polarization profiles shown in Figs. (10) and (12) generally change only slightly with

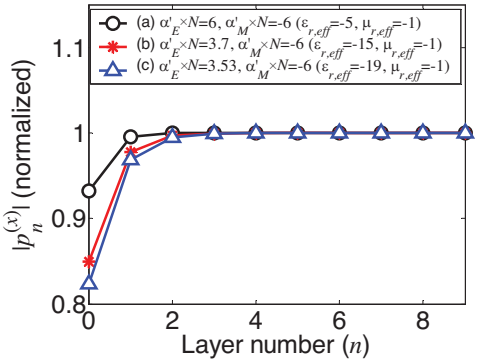

Figure 12. Polarization variation near the boundary of a semi-infinite double-negative metamaterial at planes $n = 0, 1, \ldots,$ and 9 for three different cases. $k_0 d = 0.01$.

increasing frequency. So long as $k_0 d$ is small ($k_0 d < 1$ is a good metric), the decay lengths of the extraordinary modes remain comparable, and, consequently, the polarization settles into its bulk behavior after roughly the same number of lattice planes in the direction of propagation from the boundary as shown. However, as the frequency is increased, the electrical length of this effective surface-to-bulk transition layer increases, which in turn increasingly perturbs the metamaterial's response from that found by assuming a sharp boundary and bulk behavior throughout. A more thorough investigation into the degree to which the scattering is perturbed by surface effects compared to dispersive bulk effects is reserved for future work.

10. SUMMARY AND CONCLUSIONS

In this paper we solved for the electromagnetic response of a metamaterial half-space in the case of normal incidence using an expansion of polarization in eigenmodes in the point-dipole model. Our results can be regarded as an extension of the Mahan-Obermair theory [2] to the case of a magnetodielectric crystalline structure. In our work, the problem was simplified considerably by assuming the lattice dimensions to be smaller than a half wavelength and invoking the nearest neighbor approximation. With this, we found that the metamaterial half-space supports three modes traveling in the $+z$ direction: an ordinary mode and two extraordinary modes. In the long-wavelength limit, the ordinary mode propagates with approximately

the same wave number as that predicted by effective medium theory using the Clausius-Mossotti relations, while the two extra-ordinary modes propagate with wave numbers given by Eqs. (66) and (67).

If the electric polarizability obeys condition (68) and/or the magnetic polarizability obeys condition (69), then either one or both of the extra-ordinary modes will propagate. This behavior was confirmed for a metamaterial composed of cubic particles near resonance using the Ansoft HFSS eigensolver (see Fig. 7). In this case, the structure supports multiple bulk modes even in the long-wavelength limit, and the Clausius-Mossotti relations do not present a complete description of the bulk properties of the medium.

At frequencies far removed from particle resonances, however, the extraordinary modes are evanescent and decay to zero within a few planes away from the boundary, thus giving rise to near-surface oscillations in the polarization. For such a case, the bulk of the medium can be modeled as a continuum, while the surface effects can possibly be taken into account using one of a variety models in the literature such as a thin Drude transitional layer [32], an equivalent surface conductivity [29, 33], or the generalized sheet transition conditions (GSTCs) [34, 35]. We leave the development of phenomenological models for surface effects to future work.

Our analytical solution is useful because it accounts for near-field (i.e. quasistatic) couplings between planes for metamaterials with particles exhibiting both electric and magnetic dipole responses. In this manner, our model captures detailed surface and dispersive bulk effects, which are essential for an accurate solution. Because the solution is independent of the effective medium description, it can be used as a benchmark to compare with the myriad of effective medium and surface models proposed and available in the literature. For design purposes, it is hoped that the model will promote a better understanding and insight into the scattering problem.

This work also gives insight into the problem of material parameter extraction. A common way to retrieve the material parameters of a metamaterial, based on the Nicolson-Ross retrieval algorithm for ordinary media [36], is to measure the scattering (transmission and reflection) from a finite number of cascaded planes, and infer the material parameters by assuming the structure is equivalent to an effective medium slab with sharp interfaces [1, 37]. The equations are based on the Fresnel reflection and transmission coefficients at the interface, which are in turn based on the assumption that the tangential electric and magnetic fields are continuous across the interface. This simple model, however, is in disagreement with the results of the present work and earlier works on nonmagnetic structures

(e.g., see [19, 28, 30, 38]), which find that the polarization distribution is perturbed at the surface before settling into its bulk value. Hence, one would expect the Nicolson-Ross method to present problems when applied to metamaterials, which is indeed the case. For example, the Nicolson-Ross method yields values of the retrieved material parameters that depend on the sample thickness. Specifically, as the thickness is increased, by means of adding more lattice planes to the sample, the extracted results tend to converge to some bulk value. For certain cases, convergence is reached only after three or more planes are included in the analysis [37]. This agrees, at least qualitatively, with the findings presented in Figs. 10 and 12, which suggest that the surface perturbation extends only one or two layers into the bulk for most cases of interest.

Strikingly, it has also been found that the Nicolson-Ross method applied to metamaterials sometimes produces effective permittivities and permeabilies which exhibit gain, even for passive structures (e.g., see Fig. 3 in [1] and Fig. 2 in [39]). Such non-physical artifacts are probably a result of not properly accounting for surface effects. In [40] it was recognized that the retrieval algorithm yields different results depending on the location of the effective boundaries and an attempt to solve this problem was made by choosing the appropriate location of the boundaries to that which yields a constant wave impedance (or at least as "constant" as one can achieve within some small error). While this is perhaps an improvement over earlier works, this approach still assumes the interface can be modeled by a sharp boundary. However, if quasi-static coupling between planes is non-negligible, a simple shift of reference plane does not give enough degrees of freedom to capture the surface effects, and a more complicated model is required. Additionally, it should be stressed that for cases when multiple bulk modes are present (as that shown in Fig. 11), the concept of a localized surface effect loses its meaning altogether.

REFERENCES

1. Smith, D. R., D. C. Vier, T. Koschny, and C. M. Soukoulis, "Electromagnetic parameter retrieval from inhomogeneous metamaterials," *Physical Review E*, Vol. 71, 036617(1)–036617(11), Mar. 2005.
2. Mahan, G. D. and G. Obermair, "Polaritons at surfaces," *Physical Review*, Vol. 183, 834–841, 1969.
3. Philpott, M. R., "Reflection of light by a semi-infinite dielectric," *Journal of Chemical Physics*, Vol. 60, 1410–1419, 1974.

4. Philpott, M. R., "Polaritons in a spatially dispersive dielectric half space," *Physical Review B*, Vol. 14, 3471–3487, 1976.
5. Philpott, M. R., "Effect of spatial dispersion on the S-polarized optical properties of a slab dielectric," *Journal of Chemical Physics*, Vol. 60, 2520–2529, 1974.
6. Mead, C. A., "Exactly soluble model for crystal with spatial-dispersion," *Physical Review B*, Vol. 15, 519–532, 1977.
7. Mead, C. A., "Formally closed solution for a crystal with spatial-dispersion," *Physical Review B*, Vol. 17, 4644–4651, 1978.
8. Belov, P. A. and C. R. Simovski, "Boundary conditions for interfaces of electromagnetic crystals and the generalized Ewald-Oseen extinction principle," *Physical Review B*, Vol. 73, 045102(1)–045102(14), Jan. 2006.
9. Pekar, S. I., *Crystal Optics and Additional Light Waves*, Benjamin/Cummings Pub. Co., Menlo Park, CA, 1983.
10. Tretyakov, S. A. and A. J. Viitanen, "Plane waves in regular arrays of dipole scatterers and effective-medium modeling," *Journal of the Optical Society of America A-Optics Image Science and Vision*, Vol. 17, 1791–1797, Oct. 2000.
11. Yatsenko, V. and S. I. Maslovski, "Electromagnetic interaction of parallel arrays of dipole scatterers," *Progress In Electromagnetics Research*, Vol. 25, 285–307, 2000.
12. Belov, P. A. and C. R. Simovski, "Oblique propagation of electromagnetic waves in regular 3D lattices of scatterers (dipole approximation)," *Proc. SPIE*, Vol. 4073, 266–276, 2000.
13. Belov, P. A. and C. R. Simovski, "Homogenization of electromagnetic crystals formed by uniaxial resonant scatterers," *Physical Review E*, Vol. 72, 026615(1)–026615(15), Aug. 2005.
14. Collin, R. E., *Field Theory of Guided Waves*, 2nd edition, IEEE Press, New York, 1991.
15. Simovski, C. R. and S. L. He, "Frequency range and explicit expressions for negative permittivity and permeability for an isotropic medium formed by a lattice of perfectly conducting Omega particles," *Physics Letters A*, Vol. 311, 254–263, May 12, 2003.
16. Simovski, C. R. and S. A. Tretyakov, "Local constitutive parameters of metamaterials from an effective-medium perspective," *Physical Review B*, Vol. 75, 195111(1)–195111(10), May 2007.
17. Simovski, C. R., "Analytical modelling of double-negative composites," *Metamaterials*, Vol. 2, 169–185, 2008.
18. Simovski, C. R., "Bloch material parameters of magneto-dielectric

metamaterials and the concept of Bloch lattices," *Metamaterials*, Vol. 1, 62–80, 2007.

19. Berman, D. H., "An extinction theorem for electromagnetic waves in a point dipole model," *American Journal of Physics*, Vol. 71, 917–924, Sep. 2003.
20. Wang, J. F., S. B. Qu, H. Ma, Y. M. Yang, and X. Wu, "Wide-angle polarization independent planar left-handed metamaterials based on dielectric resonators," *Progress in Electromagnetics Research B*, Vol. 12, 243–248, 2009.
21. Abramowitz, M. and I. A. Stegun, *Handbook of Mathematical Functions*, Dover Publications, Mineola, NY 1972.
22. Scher, A. D., "Boundary effects in the electromagnetic response of a metamaterial using the point-dipole interaction model," Ph.D. Dissertation, University of Colorado at Boulder, 2008.
23. Scher, A. D. and E. F. Kuester, "Extracting the bulk effective parameters of a metamaterial via the scattering from a single planar array of particles," *Metamaterials*, Vol. 3, No. 1, 44–55, 2009.
24. Sipe, J. E. and J. V. Kranendonk, "Macroscopic electromagnetic theory of resonant dielectrics," *Physical Review A*, Vol. 9, 1806–1822, 1974.
25. Jackson, J. D., *Classical Electrodynamics*, 3rd edition, Wiley, New York, 1999.
26. Kempa, K., R. Ruppin, and J. B. Pendry, "Electromagnetic response of a point-dipole crystal," *Physical Review B*, Vol. 72, 205103(1)–205103(6), Nov. 2005.
27. Brillouin, L., *Wave Propagation in Periodic Structures; Electric Filters and Crystal Lattices*, 2d edition, Dover Publications, New York, 1953.
28. Kar, N. and A. Bagchi, "Local-field effect near the surface of dipolar lattices," *Solid State Communications*, Vol. 33, 645–648, 1980.
29. Mochan, W. L. and R. G. Barrera, "Surface local field-effect," *Journal de Physique Colloque C5*, Vol. 45, 207–212, 1984.
30. Poppe, G. P. M. and C. M. J. Wijers, "Exact solution of the optical-response of thick slabs in the discrete dipole approach," *Physica B*, Vol. 167, 221–237, Dec. 1990.
31. Gadomskii, O. N. and S. V. Sukhov, "Microscopic theory of a transition layer on the ideal surface of semiinfinite dielectric media and the near-field effect," *Optics and Spectroscopy*, Vol. 89, 261–267, Aug 2000.

32. Drude, P., *The Theory of Optics*, Longmans, Green, and Co., New York, 1902.
33. Mochan, W. L. and R. G. Barrera, "Intrinsic surface-induced optical anisotropies of cubic crystals: Local field effect," *Physical Review Letters*, Vol. 55, 1192–1195, 1985.
34. Idemen, M., "Straightforward derivation of boundary-conditions on sheet simulating an anisotropic thin-layer," *Electronics Letters*, Vol. 24, 663–665, May 26, 1988.
35. Idemen, M., "Universal boundary relations of the electromagnetic-field," *Journal of the Physical Society of Japan*, Vol. 59, 71–80, Jan. 1990.
36. Nicolson, A. M. and G. F. Ross, "Measurement of intrinsic properties of materials by time-domain techniques," *IEEE Transactions on Instrumentation and Measurement*, Vol. IM-19, 377–382, 1970.
37. Smith, D. R., S. Schultz, P. Markos, and C. M. Soukoulis, "Determination of effective permittivity and permeability of metamaterials from reflection and transmission coefficients," *Physical Review B*, Vol. 65, 195104(1)–195104(5), May 15, 2002.
38. Clercx, H. J. H.and G. Bossis, "Electrostatic interactions in slabs of polarizable particles," *Journal of Chemical Physics*, Vol. 98, 8284–8293, May 1993.
39. Koschny, T., P. Markos, D. R. Smith, and C. M. Soukoulis, "Resonant and antiresonant frequency dependence of the effective parameters of metamaterials," *Physical Review E*, Vol. 68, 065602(1)–065602(4), Dec. 2003.
40. Chen, X. D., T. M. Grzegorczyk, B. I. Wu, J. Pacheco, and J. A. Kong, "Robust method to retrieve the constitutive effective parameters of metamaterials," *Physical Review E*, Vol. 70, 016608(1)–016608(7), 2004